

DESY 04-126
July 2004

A simple method for the determination of the structure of ultrashort relativistic electron bunches

E.L. Saldin, E.A. Schneidmiller, and M.V. Yurkov

Deutsches Elektronen-Synchrotron (DESY), Hamburg, Germany

Abstract

In this paper we propose a new method for measurements of the longitudinal profile of 100 femtosecond electron bunches for X-ray Free Electron Lasers (XFELs). The method is simply the combination of two well-known techniques, which were not previously combined to our knowledge. We use seed 10-ps 1047 nm quantum laser to produce exact optical replica of ultrafast electron bunches. The replica is generated in apparatus which consists of an input undulator (energy modulator), and the short output undulator (radiator) separated by a dispersion section. The radiation in the output undulator is excited by the electron bunch modulated at the optical wavelength and rapidly reaches 100 MW-level peak power. We then use the now-standard method of ultrashort laser pulse-shape measurement, a tandem combination of autocorrelator and spectrum (FROG – frequency resolved optical gating). The FROG trace of the optical replica of electron bunch gives accurate and rapid electron bunch shape measurements in a way similar to a femtosecond oscilloscope. Real-time single-shot measurements of the electron bunch structure could provide significant information about physical mechanisms responsible for generation ultrashort electron bunches in bunch compressors. The big advantage of proposed technique is that it can be used to determine the slice energy spread and emittance in multishot measurements. It is possible to measure bunch structure completely, that is to measure peak current, energy spread and transverse emittance as a function of time. We illustrate with numerical examples the potential of the proposed method for electron beam diagnostics at the European X-ray FEL.

1 Introduction

The past decade has seen tremendous progress in the development of electron accelerators that produce ultrashort bunches approaching sub-100 femtosecond durations [1,2]. The use of ultrashort electron bunches for both fundamental studies and applications is increasing rapidly, too [3–5]. As electron bunches shrink in length and grow in utility, the ability to measure them becomes increasingly important. There are several reasons for this. First, precise knowledge of the bunch properties is necessary for verifying theoretical models of bunch creation [6,7]. Second, in order to make even shorter bunches, it is necessary to understand the distortions that limit the length of currently available pulses. Third, in experiments using these bunches, it is always important to know at least the pulse length in order to determine the temporal resolution of a given experiment. Moreover, in many experiments – studies of X-ray SASE FELs, for example – additional details of the bunch structure play an important role in determination of the outcome of the experiment. Of particular importance is the variation of peak current, emittance and energy spread along the bunch. Finally, numerous applications have emerged for emittance-shaped ultrashort electron bunches and, of course, it is necessary to be able to measure the emittance, or energy spread shape of the electron bunch used in these experiments [8].

Measuring ultrashort electron bunches has always been a challenge. For five years, it was possible to create 100-fs electron bunches, but not to measure them [1,2]. Standard electron beam diagnostic tools are capable to measure bunch charge, projected emittance, and energy spread of the full electron bunch only. Unfortunately, they fail to measure the temporal dependence of the charge distribution within the bunch. It is not possible to measure slice emittance because electron bunches are so much shorter than the temporal resolution of measurement devices. Also, even when projected energy spread of the full electron bunch is measured, there is no sufficient information to determine slice energy spread and energy chirp separately. On the other hand, it is primarily the slice emittance and slice energy spread of electrons in axial slices (that are only a small fraction of the full bunch length) that determine the performance of a X-ray FEL. Thus, there is an urgent need for development of electron beam instrumentation allowing to measure bunch structure completely, that is, to measure the temporal dependence of the charge, emittance and energy spread distributions within the bunch.

The new principle of diagnostic techniques described below offers a way for full characterization of ultrashort electron bunches. It is based on a construction of an exact optical replica of an electron bunch. The replica synthesizer consists of four elements: the seed quantum laser, the modulator undulator, dispersion section, and radiator undulator. The seed laser pulse interacts with electron beam in the modulator undulator and produces the energy modulation in the

electron bunch. The electron beam then passes through the dispersion section where the energy modulation is converted to a density modulation at the optical wavelength. Particles in a modulated bunch following a second undulator radiate coherently at a wavelength of the beam density modulation. The bandwidth-limited radiation pulse has 10 μJ -level pulse energy. Longitudinal dynamics, in the undulators and dispersion section is governed by purely single-particle effects where the results do not depend on the presence of other particles. In general the radiation field depends on the peak current, local energy spread and emittance. All steps of the replica synthesis are controlled by means of the choice of the undulator parameters, dispersion section strength and value of beta function. The electric field of the wave radiated in the replica synthesizer with optimized undulator length, strength of dispersion section and focusing beta function is directly proportional to the peak current of the electron beam, $E(t) \simeq \text{const.} \times I(t)$, and does not depend on the local energy spread and emittance. So, measuring electron current profile, $I(t)$, for a single ultrashort electron pulse is reduced to the problem of a single-shot, ultrafast laser pulse-shape measurement.

To characterize such short optical pulses, conventional photodetectors and streak camera detectors do not have fast enough response times. Special measurement techniques are needed. Early on, it was realized that the only event fast enough to measure an ultrashort pulse is the optical pulse itself. A large number of clever schemes have been developed over the past twenty years to better measure ultrashort laser pulses. Most of them have been novel experimental implementations and variations of autocorrelators, but many have also offered additional information about the pulse, although never full characterization. Recently there has been a renaissance in this field and several new techniques have emerged that do achieve full characterization. They operate, not in the time or frequency domains, but in the "time-frequency domain." With the most commonly used new pulse-measurement method, frequency resolved optical gating (FROG), it is now possible to measure pulses in the visible or IR wavelength range, pulse lengths and complexities and to do so in manner that is general, robust, accurate and rigorous [9]. FROG simply involves spectrally resolving the signal beam of an intensity autocorrelator measurement. FROG is a technique to measure ultrashort laser pulses that optically constructs a spectrogram of a laser pulse. A two-dimensional (2-D) phase retrieval algorithm is used to extract the intensity and phase of a pulse from its spectrogram. The algorithm is fast enough to allow real-time inversion of the FROG spectrograms. It is also possible to measure the intensity distribution of a single ultrashort laser pulse. The entire trace can then be obtained on a single CCD camera image. Recent improvements of the FROG technique have lead to very sophisticated retrieval procedures, which can rapidly retrieve the pulse from the FROG trace. Acquisition and reconstruction rates of up to 10 Hz have been demonstrated, which makes FROG to be an ideal online tool for aligning complex femtosecond laser systems.

It is clear that the revolution that has taken place only recently in ultrashort optical pulse measurement has not only yielded powerful new laser diagnostics, but also has opened up tremendous new possibilities for ultrafast accelerator technology. With this new-found capability, a number of otherwise impossible experiments are now possible. We illustrate with numerical examples the potential of the proposed method for electron beam diagnostics at the European X-ray FEL. We demonstrate that the tandem combination of replica synthesizer and new FROG based femtosecond oscilloscope can be used to determine the temporal dependence of the charge distribution within the bunch for single ultrashort electron bunch. Proposed techniques have emerged that do achieve full characterization of the ultrashort electron bunches. The big advantage of the proposed diagnostic technique is that it can be used to determine the slice emittance and energy spread for a multishot measurements. We show that proposed technique can directly obtain the electron bunch slice energy spread and emittance from data sets of beta function and dispersion section strength scans.

2 Full characterization of femtosecond electron bunches by optical replica measurements

2.1 Optical replica synthesis

A basic scheme of the optical replica synthesizer and optical replica of a complex test electron bunch are shown in Figs. 1–3. A relatively long laser pulse is used to modulate the energy of electrons within the electron pulse at the seed laser frequency. The electron pulse will be timed to overlap with the central area of the laser pulse. The duration of the laser pulse is much larger than the electron pulse time jitter of a fraction of ps, so it can be easily synchronized with the electron pulse. The laser pulse serves as a seed for modulator which consists of a short undulator and dispersion section. Parameters of the seed laser are: wavelength 1047 nm, energy in the laser pulse 1 mJ, and FWHM pulse duration 10 ps. The laser beam is focused onto electron beam in a short (number of periods is equal to $N_w = 5$) modulator undulator resonant at the optical wavelength of 1047 nm. Optimal conditions of focusing correspond to the positioning of the laser beam waist in the center of the modulator undulator. The size of the laser beam waist is 10 times larger than the electron beam size. The seed laser pulse interacts with the electron beam in the modulator undulator and produces an amplitude of the energy modulation in the electron bunch of about 250 keV. Then the electron bunch passes through the dispersion section (momentum compaction factor is about of $R_{56} \simeq 50\mu\text{m}$) where the energy modulation is converted to the density modulation at the laser wavelength. The density modulation reaches an amplitude of about 10%. Following the modulator the beam enters the short (number of periods is equal to $N_w = 5$) radiator undulator which is resonant at laser (or double) frequency. Because

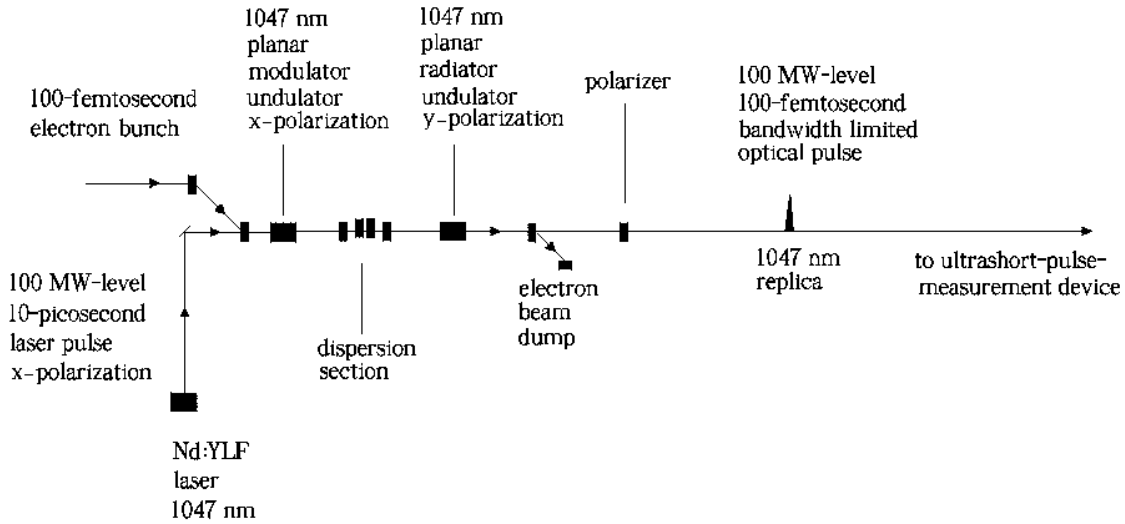


Fig. 1. Schematic diagram of the optical replica synthesis through optical modulation of electron bunch and coherent radiation in the output undulator. Signal beam filter based on polarizer: y-polarized light is transmitted, while x-polarized light is reflected

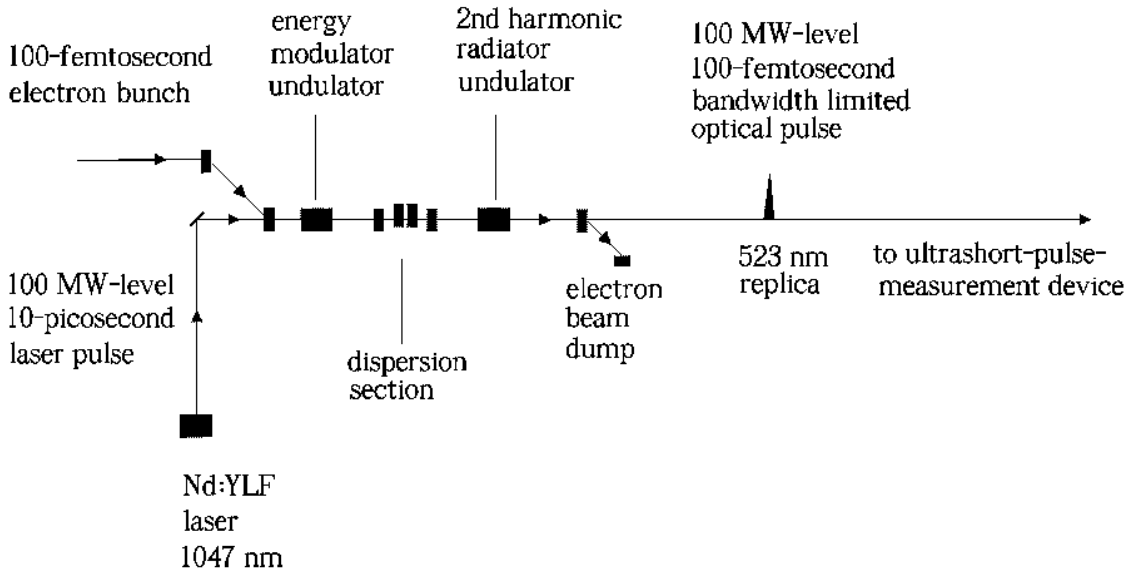


Fig. 2. Second possible schematic of replica synthesis: signal beam filter based on the 2nd harmonic generation. The bunched beam has not only a seed radiation frequency component, but also a considerable intensity in its harmonics. It is then possible to have an input undulator operating at one frequency, and an output undulator operating at double of this frequency

the beam has a large component of bunching, coherent emission is copiously produces by the electron bunch. The bandwidth-limited output radiation pulse (see Fig. 3) has 10 μ J-level pulse energy and is delivered in a diffraction-limited beam.

The optical replica synthesizer is expected to satisfy certain requirements which can be achieved by suitable design and choice of the components. A complete optimization of the proposed diagnostic device can be performed only with three-dimensional time-dependent nu-

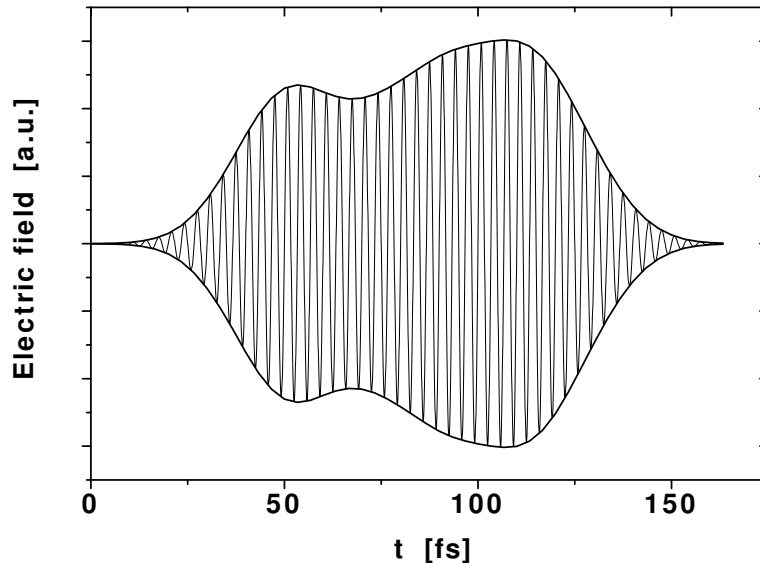


Fig. 3. Optical replica (rapidly oscillating curve) of a test electron bunch. Radiator operates at the wavelength of 1047 nm

numerical simulation code. Numerical results presented in this paper are obtained with version of code FAST [10] modified for simulation of optical replica synthesis. This code allows one to perform simulations of coherent undulator radiation taking into account all physical effects influencing the synthesizer operation.

2.1.1 Low background

One important point in the construction of replica synthesizer is separation of the optical replica from the seed laser pulse. Numerous designs are possible – for example, the combination of two planar undulators placed in crossed positions, as it is illustrated schematically in Fig. 1. Both undulators have the same period and field strength. The 1047 nm x-polarized seed radiation with 100 MW peak power and electron beam enter the first undulator, which is used to modulate the energy of electron beam. Passing the first undulator the beam and seed radiation enter the second undulator which is rotated by 90° relatively to the first undulator section. The x-polarized seed radiation does not interact with the electron beam and thus propagates freely. However, a new y-polarized radiation component is generated by the density-modulated electron beam and rapidly reaches 100 MW-level peak power. Then the electron and the light beam are separated. The electron beam is guided through a bypass and the radiation enters the polarizer which selects y-polarization. The radiation pulse after polarizer has ultrashort duration and is exact replica of the electron bunch. Finally, the radiation pulse is directed to the ultrashort-pulse-

measurement device.

In another scheme a frequency doubler is used to distinguish the optical replica from the intense seed laser pulse. The bunched beam at large values of the bunching parameter has not only a fundamental radiation frequency component, but also a considerable intensity in its harmonics. It is then possible to have an input undulator operating at one frequency, and an output undulator operating at a multiple of this frequency. The radiation in the output undulator will then be excited by the harmonic component in the electron beam, and the diagnostic instrument will operate as a frequency multiplier. A schematic diagram of the 2nd harmonic replica synthesis is shown in Fig. 2. Following the modulator the beam and seed radiation enter short undulator (radiator) which is resonant with the second harmonic of the seed radiation. In the radiator the seed radiation plays no role and is diffracted out of the electron beam, while a new 2nd harmonic radiation is generated by the density-modulated electron beam.

2.1.2 High resolution

When propagating in vacuum, the radiation field is faster than the electron beam, and it moves forward (slips) by one wavelength, λ , per one undulator period, λ_w . It is clear that the resolution of the electron pulse shape is determined by the slippage of the radiation with respect to electrons in the output undulator. If the slippage time is much less than the electron pulse duration,

$$N_w \lambda / c \ll \tau_e ,$$

then one can neglect the slippage effect. Calculation of the slippage effect shows (see Figs. 4 and 5) that this should not be a serious limitation in our case.

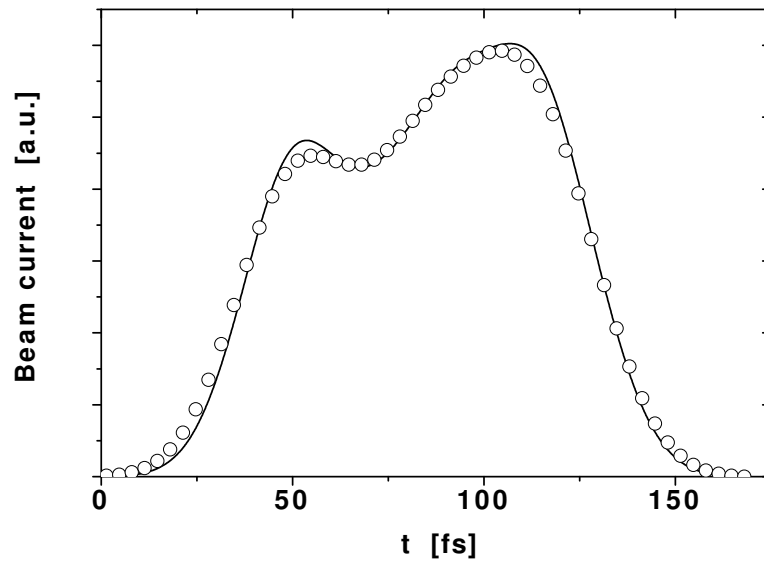


Fig. 4. Target electron beam current (solid curve) and retrieved electron pulse shape (circles) from the optical replica in Fig. 3. Number of radiator undulator periods is equal to $N_w = 5$. The optical replica is generated at the radiation wavelength 1047 nm. Discrepancies between the target and retrieved shapes are due to the slippage effect

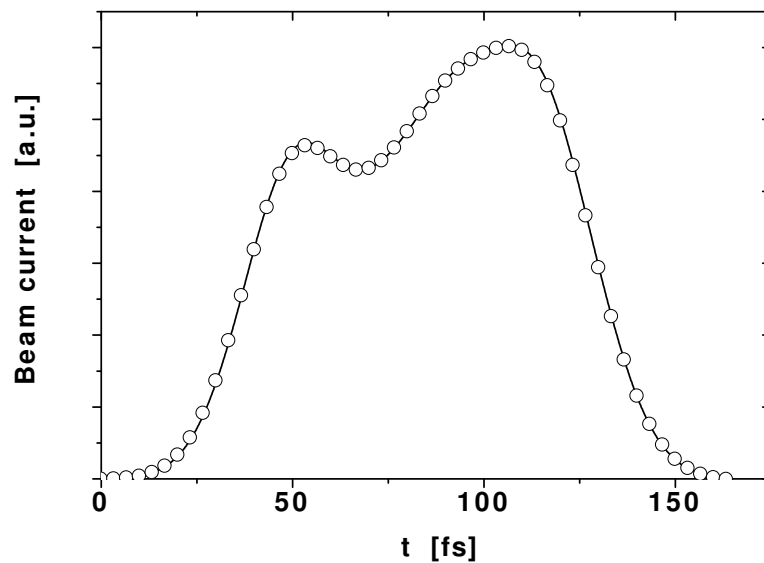


Fig. 5. Target electron beam current (solid curve) and retrieved electron pulse shape (circles) from the optical replica. Number of radiator undulator periods is equal to $N_w = 5$. The optical replica is generated at the radiation wavelength 523 nm. Note that the actual and retrieved electron bunch shapes are visually identical

2.1.3 Discussion of complicating self-interaction effects

In most applications high electron beam intensities are desired and it is therefore prudent in particular cases to test for the appearance of self-interaction effects. Proposed method for the electron pulse-shape measurement is based on the assumption that beam density modulation does not appreciably change as the beam propagates through the radiator undulator. As any oscillating charge radiates energy, so must a modulated electron beam moving along an undulator radiate energy. If the system radiates energy, then in order to preserve conservation of energy we must find that the electron beam energy is being lost. The electrons with different arrival phases acquire different values of the energy increments (positive or negative), which results in the modulation of the longitudinal velocity of the electrons with radiation frequency. Since this velocity modulation is transformed into the density modulation of the electron beam during the undulator pass, an additional radiation field exists because of variation in amplitude of density modulation. Instead, we assume that the amplitude of electron beam density modulation has the same value at all points in the undulator. This approximation means that only the contributions to the radiation field arising from the initial density modulation are taken into account, and not those arising from the induced bunching.

The problem of induced beam density modulation in the radiator undulator refers to the class of self-interaction problems. Optimization of the radiator undulator length has been performed with code FAST which takes into account collective fields (radiation and space charge fields). Typical temporal structure of electron bunches (mean energy, current, emittance and energy spread along the bunch) at the exit of the bunch compression system is presented in Fig. 6. These data sets are used as input parameters for code FAST. The smaller the number of output undulator periods, the smaller the induced density modulation and additionally smaller the slippage effect. The optimum output undulator length, keeping the resonance approximation, results in the number of periods of $N_w = 5$. Calculation shows that in this case the ratio of the induced density modulation amplitude and the initial amplitude at the output undulator exit reaches value of about a few per cent only. Thus we find that collective effects in the output undulator are not important in our case.

Longitudinal beam dynamics in the modulator undulator as assumed in this paper is governed by purely single-particle effects where the results do not depend on the presence of other particles. During the passage through a modulator the electron density modulation at the optical wavelength can be perturbed by the collective fields. As a result, the small induced bunching requirement dictates the use of modulator undulator length to be of a few periods only. In the case under study, the optimum number of the modulator undulator periods is equal to $N_w = 5$.

The next problem to be studied is that of estimating the collective effects influencing the operation of dispersion section. Particles in a modulated bunch following a curved path may

radiate coherently at a wavelength of the beam density modulation. When an electron bunch passes the dispersion section, radiative interaction induces an additional density modulation. The design of modulator chicane is based on the need to minimize coherent synchrotron radiation (CSR) induced microbunching. The problem connected with radiative interaction of the particles in the bunch with sinusoidal density excitation moving in a magnetic chicane has been investigated analytically and numerically [11–13]. Calculation of the CSR effects shows that this should not be a serious limitation in our case.

2.1.4 *The method of obtaining information about electron current profile*

The study and detailed understanding of the cause and nature of collective effects is important for successful design of replica synthesizer. Proposed design is conducted to eliminate collective effects as much as possible through installation of short input and output undulators. The signal produced by replica synthesizer is thus a pulse of electric field amplitude:

$$E(t) = F(I(t), \epsilon_n(t), \Delta\mathcal{E}(t)) = I(t)f(\epsilon_n(t), \Delta\mathcal{E}(t)) ,$$

where $\epsilon_n(t)$ is the normalized slice emittance and $\Delta\mathcal{E}(t)$ is the slice energy spread in the electron bunch. If longitudinal beam dynamics in the synthesizer is governed by purely single-particle effects then this field directly proportional to the peak current $I(t)$.

Within the scope of the electrodynamic theory the output characteristics of the replica synthesizer are controlled by three dimensional parameters: λ , L_w , σ , where λ is the radiation wavelength, $L_w = N_w \lambda_w$ is the radiator undulator length, and σ is the electron beam transverse size. At an appropriate normalization of electrodynamic equations, the coherent undulator radiation is described by only one dimensionless parameter:

$$N = 2\pi\sigma^2/(\lambda L_w) .$$

The parameter N can be referred to as the electron beam Fresnel number, or as diffraction parameter. In general case the electric field of the wave radiated in the undulator depends on the transverse size of the electron beam. For a proposed diagnostic technique it is of great interest to minimize the influence of the transverse emittance on the radiation field amplitude. In the case of a wide electron beam

$$\lambda L_w \ll 2\pi\sigma^2 , \quad \text{or} \quad N \gg 1 , \tag{1}$$

the most of the radiation overlaps with electron beam and field of the wave is inversely proportional to the square of electron beam

$$E(t) \propto I(t)/\sigma^2(t) .$$

Reducing the particle beam cross-section by diminishing the betatron function reduces also the size of the radiation beam and increases the total power of output radiation. This process of reducing the beam cross-section is, however, effective only up to some point. Further reduction of the particle beam size would practically no effect on the radiation beam size and total radiation power because of diffraction effects (see Section 4). In the limit of a thin electron beam the transverse radiation beam size tends to the constant value and the dependence of the output radiation on the transverse size of the electron beam is rather weak. The boundary between these two asymptotes is about $\sigma^2 \simeq \lambda L_w$.

From the preceding discussion we may want to optimize the beam geometry as follows. The transverse size of the electron beam has to be much smaller than the diffraction limited radiation beam size

$$\sigma^2 \ll \lambda L_w / (2\pi), \quad \text{or} \quad N \ll 1, \quad (2)$$

The radiation wavelength and the undulator length dictate the choice of the optimum transverse size of the electron beam. Let us present a specific numerical example. Suppose $\gamma = 10^3$, $\epsilon_n = 2\pi\mu\text{m}$, $\lambda_w = 6.5\text{ cm}$, $N_w = 5$, $\lambda = 1\mu\text{m}$. If the focusing beta function is equal to 1 m the diffraction parameter is $N = 2\pi\sigma^2/(\lambda L_w) \simeq 0.04$. We come to the conclusion that we can treat this situation as a coherent undulator radiation generated by a thin electron beam. This condition may be easily satisfied in practice.

Proposed design is conducted to eliminate emittance effects as much as possible through installation of a special electron beam focusing system. In the radiator undulator the betatron function should reach small values (of about 1 m) forming a narrow beam waist. The signal generated by a replicas synthesizer is thus a pulse of electric field with amplitude:

$$E(t) = F(I(t), \epsilon_n(t), \Delta\mathcal{E}(t)) = I(t)f(\Delta\mathcal{E}(t)).$$

Optimum parameters of the dispersion section can be estimated in the following way. The expression for the fundamental component of the bunched beam current is $i_1(t) = 2I(t)J_1(X)$, where $X = 2\pi R_{56}\delta\mathcal{E}/(\lambda\mathcal{E}_0)$ is dimensionless quantity known as the bunching parameter, $\delta\mathcal{E}$ is the amplitude of energy modulation induced in the modulator undulator. The function $J_1(X)$ approaches $X/2$ for small X ; thus the microbunching approaches $i_1(t) \simeq XI(t)$. We see that microbunching depends on the choice of the dispersion section strength. One might think that all we have to do is to get microbunching amplitude to maximum – we can always increase R_{56} of the dispersion section and we can always increase output power. It is not impossible to build dispersion section that has large R_{56} function. In fact, one of the main problems in the modulator operation is preventing the spread of microbunching due to local energy spread in the electron beam. For effective operation of replica synthesizer the value of suppression factor

should be close to unity. To get a rough idea of the spread of electron density modulation, the position of the particles within the electron beam at the dispersion section exit has a spread which is equal to $\Delta z' \simeq R_{56} \Delta \mathcal{E} / \mathcal{E}_0$, where $\Delta \mathcal{E}$ is the local energy spread in the electron bunch. We know that uncertainty in the phase of the particles is about $\Delta \psi \simeq 2\pi \Delta z' / \lambda$. Therefore, a rough estimate for the microbunching spread to be small is

$$2\pi R_{56} \Delta \mathcal{E} / \mathcal{E}_0 \ll 1. \quad (3)$$

The result of more careful analysis (see Section 3) shows that in our case the optimal condition can be written as $X \simeq 0.1$, $\delta \mathcal{E} \simeq \max(\Delta \mathcal{E}) / 3 \simeq 250$ keV. The amplitude of energy modulation dictates the choice of the seed laser parameters. In our case the optimal peak power of the seed laser is about of 100 MW.

In general, radiation field depends on the peak current, $I(t)$, local energy spread, $\Delta \mathcal{E}(t)$, and local emittance, $\epsilon_n(t)$. However, under conditions of a thin electron beam (2) and of a microbunching spread to be small (3), the electric field of the wave radiated in the replica synthesizer is directly proportional to the peak current of the electron beam:

$$E(t) = F(I(t), \epsilon_n(t), \Delta \mathcal{E}(t)) = \text{const.} \times I(t).$$

Thus, conditions (2) and (3) should be treated as optimal tuning of undulator length, strength of the dispersion section and focusing beta function for measurement of the electron bunch profile.

2.1.5 *The method of obtaining information about slice emittance and energy spread*

We found that longitudinal profile of the electron bunch $I(t)$ can be reconstructed on the basis of a single-shot measurements. The next problem is determination of slice energy spread ($\Delta \mathcal{E}(t)$) and slice emittance ($\epsilon_n(t)$). This can be done on the basis of multishot measurements. If the electron pulse shape, $I(t)$, is known, the local energy spread $\Delta \mathcal{E}(t)$ can be determined from the dispersion section strength scan. In this way, the problem of slice energy spread measurement is transformed into a relatively simple task of measuring the radiation field amplitude maximum ($\max E(t) \propto \max i_1(t)$). An attempt to increase of the amplitude of the fundamental harmonic, by increasing the strength of dispersion section, is countered by decrease the energy spread suppression factor. In Section 3 we demonstrate that the microbunching $i_1(t)$ has clearly a maximum

$$\max i_1(t) = \text{const.} \times \delta \mathcal{E}[I(t) / \Delta \mathcal{E}(t)],$$

and the optimum strength of the dispersion section is

$$R_{56} = \frac{\lambda \mathcal{E}_0}{2\pi \Delta \mathcal{E}(t)} .$$

Thus, measuring the $\max E(t)$ is strictly equivalent to measuring the local energy spread variations along the electron bunch:

$$I(t)/[\max E(t)] = \text{const.} \times \Delta \mathcal{E}(t) .$$

Since the optimal strength of the dispersion section is known, that of the unknown absolute value of slice energy spread, $\Delta \mathcal{E}(t)$, is easily found too.

Slice emittance can be measured in the following way. Let us consider for illustration of the method a simple model of the electron bunch, assuming that slice emittances are different, but Twiss parameters are the same in all slices (more general model is discussed in section 5). The solution in our case is to realize that in a wide electron beam asymptote (1) the most of the radiation overlaps with the electron beam and the field of the wave is inversely proportional to the square of the electron bunch, $E(t) \propto I(t)/\sigma^2(t)$. If the electron pulse shape, $I(t)$, is known, the problem of the slice emittance measurement is transformed into a simple task of measuring the radiation field amplitude in the case of a wide electron beam

$$I(t)/E(t) = \text{const.} \times \sigma^2(t) \quad \text{as} \quad \min(\sigma^2) \gg \lambda L_w / (2\pi) .$$

Since the value of beta function and projected emittance are known (from a standard method using a screen and quadrupole scan), then the unknown absolute value of slice emittance $\epsilon_n(t)$ is easily determined, too.

We illustrate retrieval of the slice bunch properties from the optical replica of the electron bunch. We take two different electron bunches (right and left columns in Fig. 6), and perform numerical calculations using code FAST. The nominal energy of electrons is equal to $\mathcal{E}_0 = 500$ MeV. Number of undulator periods in the modulator and radiator undulator is equal to $N_w = 5$. Period length is 6.5 cm. The optical replica is generated at the radiation wavelength 1047 nm. The seed laser power is 100 MW, FWHM pulse duration is 10 ps. Upper plots in Fig. 6 show comparison of target and reconstructed values for the beam current. When taking these data, parameters for the numerical experiment were set according to conditions (2) and (3): focusing beta function in the radiator is 1 meter, and net compaction factor of the dispersion section is 50 μm . Calculations show that pulse energy in the optical replica exceeds 30 μJ . Slice energy spread was determined by means of the scan of dispersion section strength at the value of beta-function of 1 meter (lower plots in Fig. 6). The values of slice emittance were extracted with the help of additional set of calculations with large value of beta function of 50 m which corresponds

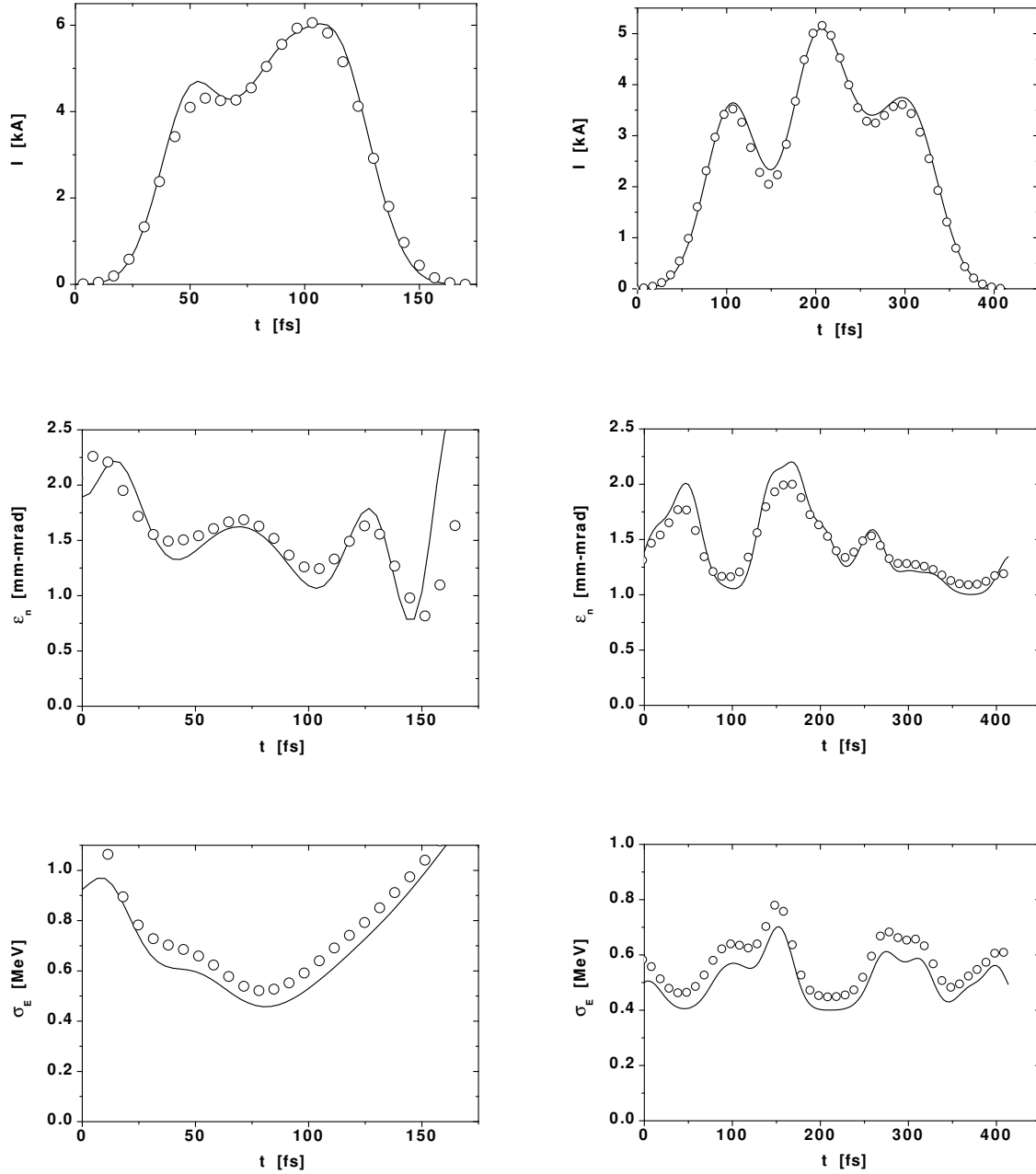


Fig. 6. Target (solid curve) and retrieved (circles) electron beam peak current, slice emittance and slice energy spread. Two different test electron pulses are used in the optical replica calculations (right and left columns). The nominal energy of electrons is equal to $\mathcal{E}_0 = 500$ MeV. Number of undulator periods is equal to $N_w = 5$. The optical replica is generated at the radiation wavelength 1047 nm

to the limit of a wide electron beam. We see that slice bunch properties can be retrieved with high accuracy if optical replica can be characterized with high accuracy. The latter problem is the subject of the next section.

There is no doubt that numerical simulation code gives a correct prediction for a given set of parameters. However, in many cases a more transparent physical analysis would be more preferable. The calculation scheme of the replica characteristics which is suitable for engineering practice is presented in Sections 3 and 4. This scheme stems from similarity techniques and numerical calculation results given as universal plots. It may be especially useful at the design stage of an experiment. To concentrate on the diffraction effects, in Section 4 we have restricted our attention to the steady-state theory of the coherent undulator radiation. We assumed that a continuous electron beam with current density constant in time is fed to the undulator entrance. In practical situations the electron beam has a finite pulse duration (about 100 fs), and the question arises of when one can use the results of Section 4. If the slippage time of the radiation with respect to electrons per undulator length is much less than the electron pulse duration, then one can neglect the slippage effects and use the steady-state approach. Now let us consider the electron pulse with the gradient axial profile of current $I(t)$. As an approximation, the smooth profile $I(t)$ may be replaced by a "boxcar" function. The pulse duration interval is divided into N_s subintervals of equal length. Within each subinterval, the approximation to $I(t)$ is constant. At the end of the each subinterval, the approximate profile jumps to a new constant value. When $N_w \lambda / c < \tau_e / N_s$ we can calculate the coherent undulator radiation separately within each subinterval. Using the plots presented in Fig. 4 and Fig. 5, one can give a quantitative answer to the question about the region of applicability of the steady-state model.

2.2 *Ultrashort optical pulse-shape measurements using frequency-resolved optical gating*

The shape of the electron bunch replica cannot be measured using even the fastest photodiodes or streak camera detectors. The rise time of the best streak-cameras approaches 0.1 picosecond, far too slow to resolve the femtosecond structure of ultrafast optical pulses. Early on, it was realized that the only event fast enough to measure an ultrashort pulse is the pulse itself. This gave birth to the now-standard method of measurement: the intensity autocorrelation (AC). Specifically, it involves splitting the pulse into two, variably delaying one with respect to the other, and spatially overlapping the two pulses in some instantaneously responding nonlinear-optical medium, such as second-harmonic-generation (SHG) crystal. A SHG crystal produces light at a twice the frequency of input light with an intensity that is proportional to the product of the intensities of the two input pulses. It is clear that this yields some measure of the pulse length because no second harmonic intensity will result if the pulses do not overlap in time. Thus, a relative delay of one pulse length will typically reduce the SHG intensity by about a factor of two.

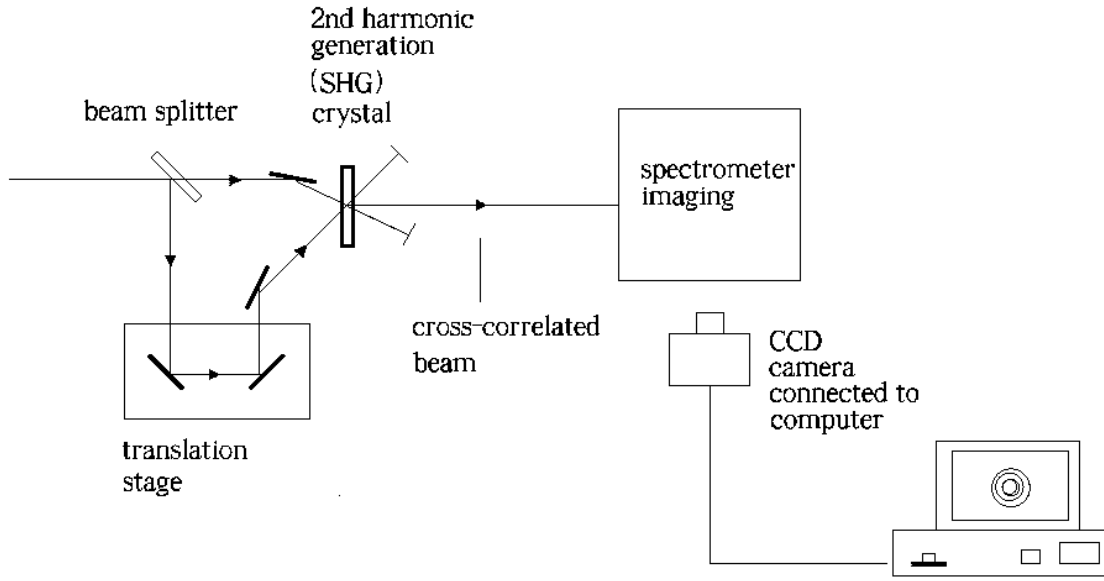


Fig. 7. A schematic of ultrashort-pulse-measurement device – SHG FROG, the most common and most sensitive version of FROG. Like in the autocorrelation device the two beams are combined in the SHG crystal and a frequency doubled signal beam is created. This signal beam is then sent through an imaging spectrometer which outputs the beam frequency as a function of a distance. The output of the spectrometer (the FROG trace, or spectrogram) is captured by a CCD camera. The pulse shape is then determined using an algorithm in a computer connected to the camera

Mathematically, the autocorrelation $A(\tau)$ is given by:

$$A(\tau) = \int_{-\infty}^{\infty} I(t)I(t + \tau) dt .$$

One immediately recognizes the physical meaning of the autocorrelation function. The Fourier transform of the autocorrelation is $\bar{A}(\omega)$, related to the Fourier transform of the signal by: $\bar{A}(\omega) = |\bar{I}(\omega)|^2$. An autocorrelation is always a symmetric function. The Fourier transform of the autocorrelation is a real function, consistent with a symmetric function in the time domain. The question then naturally arises as to exactly what information about $I(t)$ can be derived from the measurement of cross-correlation. One can see that the correlation technique provides the possibility to measure the modulus of the Fourier transform of the signal function, while information about its phase is missing. Also, even when the spectrum is also measured there is not sufficient information to determine the pulse. Despite these serious drawbacks, the autocorrelation and spectrum have remained the standard measures of ultrashort pulses for over 20 years, largely for lack of better methods [14].

The problem of ultrafast-pulse measurements have recently been solved. The autocorrelator and spectrum are the building blocks for a new pulse-shape measurement technique, frequency resolved optical gating (FROG), which is simply the spectrum of autocorrelation [9]. A tandem

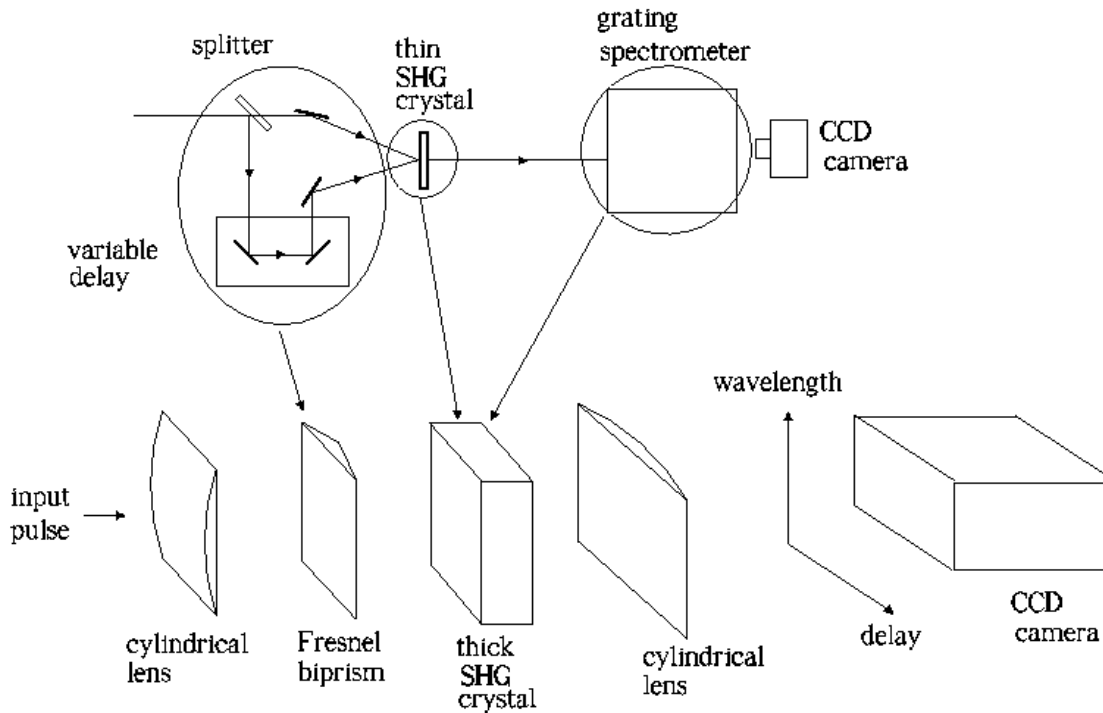


Fig. 8. A schematic of a single-shot FROG trace measurement device. FROG trace can be produced by a device composed of a few as five simple optical elements. GRENOUILLE is the simplest ultrashort-pulse measurement device in the history. This trivial device uses a Fresnel biprism to replace the beam splitter, delay line, and beam-recombining optics. It maps delay to position at the crystal. GRENOUILLE also utilizes a thick SHG crystal acting as both the non-linear-optical time-gating element and the spectrometer. A complete single-shot SHG FROG trace results. Whereas an autocorrelator (see top) has four sensitive alignment parameters, GRENOUILLE has no sensitive alignment parameters at all

combination of autocorrelator and spectrum can be used to extract shape information from ultrashort pulses. The technique is applicable to single-shot measurements. Although there are many different types of FROG's the type of geometry we will focus on what is known as the Second Harmonic Generation (SHG) FROG (see Fig. 7). Under this FROG geometry, a SHG crystal is used just like in the autocorrelation device to resolve the time axis, but additionally the signal beam is sent through an imaging spectrometer, which uses diffraction gratings to separate the light of the signal beam, in effect spatially representing the frequency of the signal beam. The spectrometer outputs to camera the images of the signal beam after they have been separated into its component wavelengths, known as FROG traces. To retrieve pulse-shape information the trace is sent through FROG algorithm, which uses constraints to iterate to a unique solution for both the phase and intensity of the pulse as a function of time. The intensity as a function of time will give us the structure of the electron bunch.

Measurement of a spectrogram, that is, the Fourier transform of a function of two variables, thus frames the ultrashort-pulse measurement problem in a form that allows a rigorous and general solution. This realization lead to the introduction of iterative inversion algorithms. The

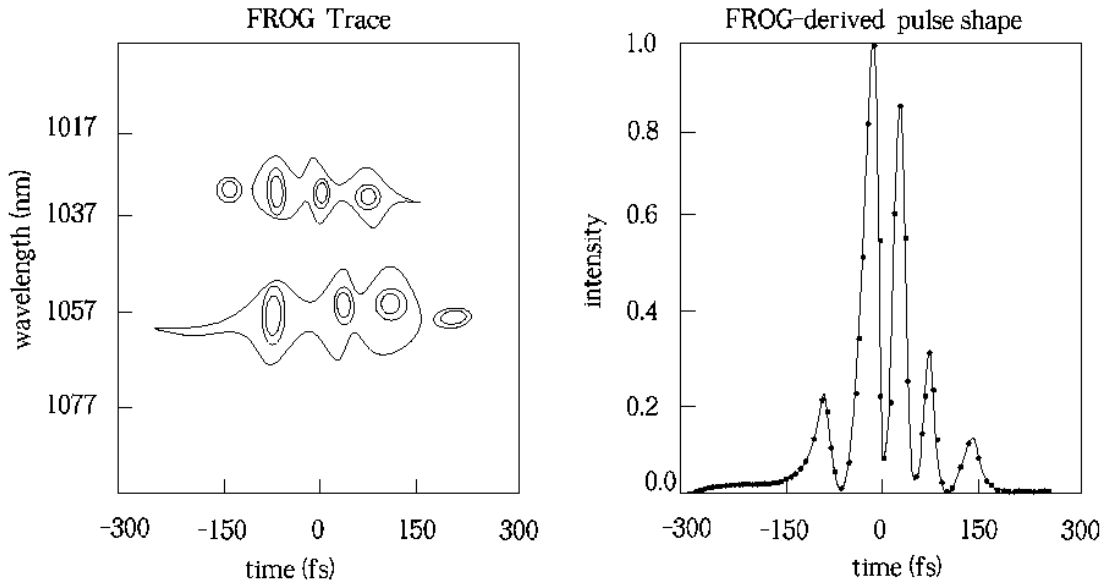


Fig. 9. Front panel display of the femtosecond oscilloscope. The device can display the pulses inverted by an iterative algorithm at a rate of 10 Hz

important point is that any algorithm that takes into account all the $N \times N$ data points of the spectrogram, rather than N data points in the time domain and N data points in the frequency domain, produces a better estimate of the pulse, since it has much more materials with which to work. The problem of determining the pulse intensity and phase from spectrogram is essentially equivalent to the two-dimensional "phase retrieval" problem in image science. Phase retrieval is the problem of finding a function knowing only the magnitude (but not the phase) of its Fourier transform. Phase retrieval for a function of one variable is impossible. For example, knowledge of a pulse spectrum does not fully determine the pulse – many different pulses have the same spectrum. But image scientists found that phase retrieval for a function of two variables is possible. Knowledge of only the magnitude of a two-dimensional Fourier transform of a function of two variables essentially uniquely determines the function provided that the function is of finite extent.

Quite surprisingly, a FROG trace of a pulse can be produced by an almost trivial device composed of as few as five simple optical elements. This extremely simple device is called GRENOUILLE [15]. It involves replacing the beam splitter, delay line, and beam combining optics with a simple element, a Fresnel biprism (a prism with an apex angle close to 180°). When a Fresnel biprism is illuminated with a wide beam, it splits the beam into two beamlets and crossed them at an angle yielding interference fringes. While fringes aren't relevant to pulse measurement, crossing beams at an angle is exactly what is required in conventional single-shot autocorrelator and FROG beam geometries, in which the relative beam delay is mapped onto horizontal position at the crystal (see Fig. 8). Beams that are split and crossed by a Fresnel

biprism are automatically aligned in space and in time, which is a significant simplification with respect to conventional geometries. GRENOUILLE uses a thick SHG crystal, which not only gives considerably more signal (signal strength scales as the approximate square of the thickness), but also simultaneously replaces the spectrometer. It operates as a single-shot device. GRENOUILLE involves no beam-splitting, no beam-recombining, and no scanning of the delay, and so has zero sensitive alignment degrees of freedom. Two additional cylindrical lenses complete the device. The first cylindrical lens must focus the beam into the thick crystal tightly enough to yield a range of crystal incidence (and hence exit) angles large enough to include the entire spectrum of the pulse. After the crystal, a cylindrical lens then maps the crystal exit angle onto position at the camera, with the wavelength as a near-linear function of (vertical) position.

This device is capable of measuring complex pulses. This is because a FROG traces large number of points (about 10 thousands in a 100×100 trace) giving sufficient information capacity to measure a pulse with a large amount of structure. It is also possible to measure the intensity distribution of a single ultrashort laser pulse. The entire trace can then be obtained on a single camera image. An iterative phase-retrieval algorithm is used to find the pulse field for a given trace. This algorithm works well and generally converges in a 0.1 second or so at modern CPUs. The front panel of such femtosecond oscilloscope is shown in Fig. 9.

3 Operation of the optical modulator

The optical modulator consists of three elements: the optical seed laser, the modulator undulator, and the dispersion section. The seed laser pulse interacts with the electron beam in the modulator undulator which is resonant with the laser frequency ω , and produces the energy modulation in the electron bunch (see Fig. 10). The electron beam then passes through the dispersion section where the energy modulation is converted to a density modulation at the optical wavelength. The dispersion section is designed to introduce the energy dependence of the particle's path length, $\Delta z = R_{56} \delta \mathcal{E} / \mathcal{E}_0$. Several designs are possible, but the simplicity of a four-dipole magnet chicane is attractive because it adds no net beamline bend angle or offset and allows simple tuning of the momentum compaction factor, R_{56} , with a single power supply (see Fig. 11). The trajectory of the electron beam in the chicane has the shape of an isosceles triangle with base length L . The angle adjacent to the base, θ_B , is considered to be small. For ultra-relativistic electrons and small bend angles, the net compaction factor R_{56} of the chicane is given by

$$R_{56} = L\theta_B^2 .$$

Let us consider operation of the dispersion section. The phase space distribution of the particles in the first undulator is described in the terms of distribution function $f(P, \psi)$ written in "energy-phase" variables $P = \mathcal{E} - \mathcal{E}_0$ and $\psi = 2\pi z'/\lambda' = \omega(z/v_z - t)$, where \mathcal{E}_0 is the nominal energy of the particle and ω is the angular frequency. Before entering the first undulator, the electron energy distribution is assumed to be Gaussian:

$$f_0(P) = \frac{1}{\sqrt{2\pi\langle(\Delta\mathcal{E})^2\rangle}} \exp\left(-\frac{P^2}{2\langle(\Delta\mathcal{E})^2\rangle}\right).$$

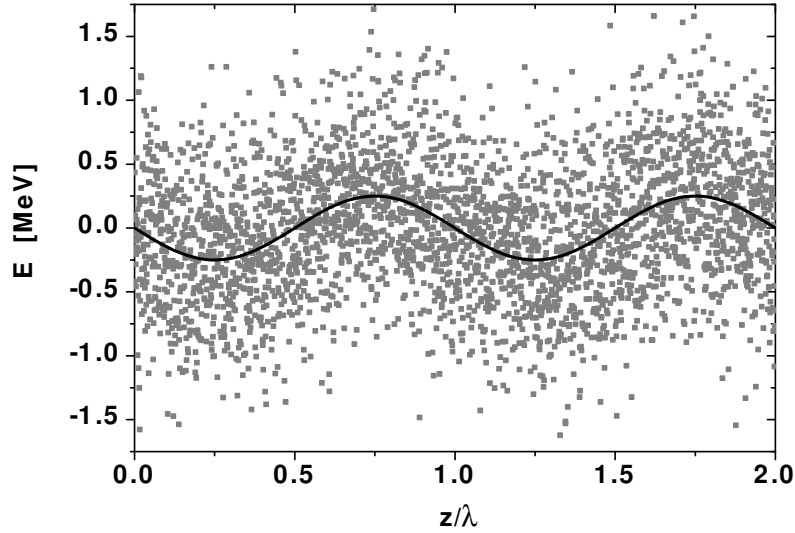
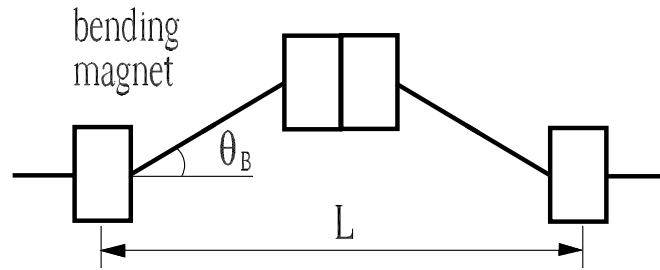


Fig. 10. Phase space distribution of electrons at the exit of the modulator undulator. Solid line shows laser induced energy modulation



$$R_{56} = L\theta_B^2$$

Fig. 11. Schematic of dispersion section

The present study assumes the density modulation at the end of the modulator undulator to be very small, and there is an energy modulation $P_0 \sin \psi$ only. Then the distribution function at the entrance to the dispersion section is

$$f_0(P - P_0 \sin \psi) .$$

After passing through the dispersion section with dispersion strength $d\psi/dP$, the electrons of phase ψ and energy deviation P will come to the new phase $\psi + P d\psi/dP$. Hence the distribution function becomes

$$f(P, \psi) = f_0 \left(P - P_0 \sin \left(\psi - P \frac{d\psi}{dP} \right) \right) .$$

The dispersion strength parameter and compaction factor are connected by the relation

$$\frac{d\psi}{dP} = \frac{2\pi}{\lambda'} \frac{dz'}{d\mathcal{E}_0} = \frac{2\pi}{\lambda'} \frac{R_{56}}{\mathcal{E}_0} .$$

The integration of the phase space distribution over energy provides the beam density distribution, and the Fourier expansion of this function gives the harmonic components of the density modulation converted from the energy modulation [16]. At the dispersion section exit, we may express current I in the form

$$\begin{aligned} I &= I_0 \int_{-\infty}^{\infty} f(P, \psi) dP = I_0 + 2I_0 \sum_{n=1}^{\infty} \exp \left[-\frac{1}{2} n^2 \langle (\Delta\mathcal{E})^2 \rangle \left(\frac{d\psi}{dP} \right)^2 \right] \\ &\times J_n \left(nP_0 \frac{d\psi}{dP} \right) \cos(n\psi) . \end{aligned} \quad (4)$$

We find a set of harmonic waves, of which the fundamental term, with angular frequency ω , is the one of importance in a radiator. This fundamental term involves the phase variation $\cos \psi$, and an amplitude term

$$a_1 = 2J_1 \left(P_0 \frac{d\psi}{dP} \right) \exp \left[-\frac{1}{2} \langle (\Delta\mathcal{E})^2 \rangle \left(\frac{d\psi}{dP} \right)^2 \right] . \quad (5)$$

For small input signal we may assume that the argument of the Bessel function is small. The function $J_1(X)$ approaches $X/2$ for small X , thus the microbunching approaches

$$a_1 = P_0 \frac{d\psi}{dP} \exp \left[-\frac{1}{2} \langle (\Delta\mathcal{E})^2 \rangle \left(\frac{d\psi}{dP} \right)^2 \right] .$$

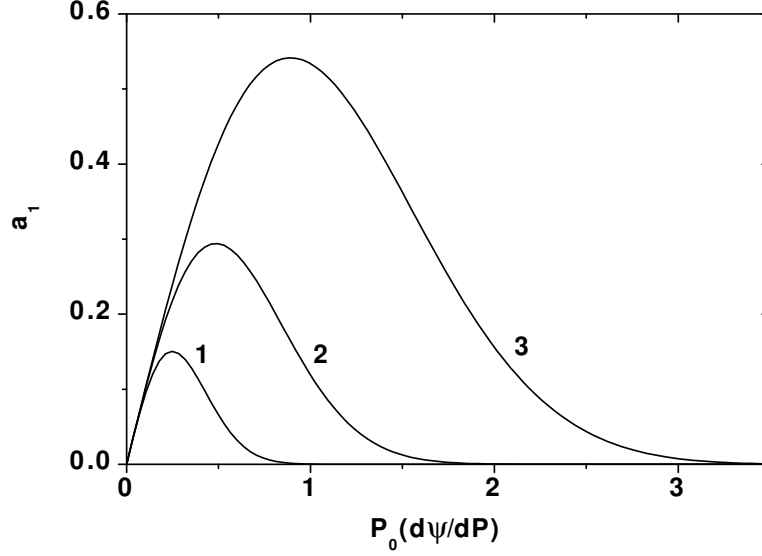


Fig. 12. Dependence of a_1 , fundamental component of bunched beam current, on bunching parameter $X = P_0 d\psi/dP$ and on the parameter $P_0/\sqrt{\langle(\Delta\mathcal{E})^2\rangle}$ giving the relative amplitude of beam energy modulation. Curve 1: $P_0/\sqrt{\langle(\Delta\mathcal{E})^2\rangle} = 0.25$. Curve 2: $P_0/\sqrt{\langle(\Delta\mathcal{E})^2\rangle} = 0.5$. Curve 3: $P_0/\sqrt{\langle(\Delta\mathcal{E})^2\rangle} = 1$

The relation between a_1 and bunching parameter for different values of energy spread is shown in Fig. 12. We see that microbunching depends greatly on the choice of the dispersion section strength. An attempt to increase the amplitude of the fundamental harmonic by increasing the strength of dispersion section, is countered by a decrease of the exponential factor. The microbunching a_1 has clearly a maximum

$$(a_1)_{\max} = \frac{P_0}{\sqrt{2.72\langle(\Delta\mathcal{E})^2\rangle}},$$

and the optimum strength of the dispersion section is

$$\left(\frac{d\psi}{dP}\right)_{\max} = \frac{1}{\sqrt{\langle(\Delta\mathcal{E})^2\rangle}}.$$

Let us consider numerical example for $P_0 = 250$ keV, $\sqrt{\langle(\Delta\mathcal{E})^2\rangle} = 500$ keV, $\mathcal{E}_0 = 500$ MeV, and $\lambda = 1047$ nm. The calculation gives $a_1 = 0.1$ at $R_{56} = 30\mu\text{m}$. The suppression factor in (5) is equal to $\exp[-\omega^2\langle(\Delta\mathcal{E})^2\rangle R_{56}^2/(2c^2\mathcal{E}_0^2)] \simeq 0.98$. We come to the conclusion that we can treat this situation as an optimum modulator design. The optimum condition for the replica synthesis is that the modulator should present a rather weak dependence of the output modulation on the local energy spread in the electron beam.

4 Operation of the optical radiator

Proposed technique of electron bunch diagnostics essentially exploits the properties of the radiation generated by modulated electron beam in the undulator. To simplify consideration we start with the case of a helical undulator. Later on all the results will be generalized for the case of a planar undulator. The magnetic field on the axis of the helical undulator is given by

$$\vec{H}_w = \vec{e}_x H_w \cos(k_w z) - \vec{e}_y H_w \sin(k_w z) ,$$

where $k_w = 2\pi/\lambda_w$ is the undulator wavenumber and $\vec{e}_{x,y}$ are unit vectors directed along the x and y axes of the Cartesian coordinate system (x, y, z) . The Lorentz force $\vec{F} = -e(\vec{v} \times \vec{H}_w)/c$ is used to derive the equations of motion of electrons with charge $(-e)$ and mass m_e in the presence of the magnetic field. The explicit expression for the electron velocity in the field of the helical undulator has the form:

$$\vec{v}_\perp(z) = c\theta_w[\vec{e}_x \cos(k_w z) - \vec{e}_y \sin(k_w z)] ,$$

which means that the electron in the undulator moves along a constrained helical trajectory parallel to the z axis. The angle of rotation is given by the relation $\theta_w = K/\gamma = \lambda_w e H_w / (2\pi m_e c^2 \gamma)$, where $\gamma = (1 - v^2/c^2)^{-1/2}$ is the relativistic factor and $v^2 = v_x^2 + v_y^2 + v_z^2$. As a rule, the electron rotation angle θ_w is small and the longitudinal electron velocity v_z is close to the velocity of light, $v_z \simeq c$.

Let us consider periodically modulated relativistic electron beam moving along the z axis in the field of a helical undulator. In what follows we use the following assumptions: i) electrons move along constrained helical trajectories in parallel with the z axis; ii) the radius of the electron rotation in the undulator, $r_w = \theta_w/k_w$, is much less than the transverse size of the electron beam; iii) electron beam density at the undulator entrance is simply $n = n_0(\vec{r}_\perp)[1 + a_{\text{in}} \cos \omega(z/v_z - t)]$, where $a_{\text{in}} = \text{const}$. In other words we consider the case in which there are no variations in amplitude and phase of the density modulation in the transverse plane. Under this assumptions the transverse current density may be written in the form

$$\vec{j}_\perp = -e\vec{v}_\perp n(\vec{r}_\perp, z/v_z - t) = -e\vec{v}_\perp n_0(\vec{r}_\perp)[1 + a_{\text{in}} \cos \omega(z/v_z - t)] ,$$

where we calibrated the time in such a way that current density has its maximum at time $t = 0$, at point $z = 0$. Even though the measured quantities are real, it is more convenient to use complex representation. For this reason, starting with real \vec{j}_\perp , one defines the complex transverse current density:

$$j_x + i j_y = -ec\theta_w n_0(\vec{r}_\perp) \exp(-i k_w z) [1 + a_{\text{in}} \cos \omega(z/v_z - t)] . \quad (6)$$

Transverse current have the angular frequency ω and two waves travelling in the same direction with variations $\exp i(\omega z/v_z - k_w z - \omega t)$ and $\exp -i(\omega z/v_z + k_w z - \omega t)$ will add to give a total current proportional to $\exp(-i k_w z) \cos \omega(z/v_z - t)$. The factor $\exp i(\omega z/v_z - k_w z - \omega t)$ indicates a fast wave, while the factor $\exp i(\omega z/v_z + k_w z - \omega t)$ indicates a slow wave. The use of the word "fast" ("slow") here implies a wave with phase velocity faster (slower) than the beam velocity.

Now we should consider the electrodynamic problem. Using Maxwell's equations, we can write the equation for the electric field

$$c^2 \vec{\nabla} \times (\vec{\nabla} \times \vec{E}) = -\partial^2 \vec{E} / \partial t^2 - 4\pi \partial \vec{j} / \partial t .$$

Then we make use of the identity

$$\vec{\nabla} \times (\vec{\nabla} \times \vec{E}) = \vec{\nabla}(\vec{\nabla} \cdot \vec{E}) - \vec{\nabla}^2 \vec{E} ,$$

where $\vec{\nabla} \cdot \vec{E}$ can be found from the Poisson equation. Finally, we come to the inhomogeneous wave equation for \vec{E} :

$$c^2 \vec{\nabla}^2 \vec{E} - \partial^2 \vec{E} / \partial t^2 = 4\pi c^2 \vec{\nabla} \rho + 4\pi \partial \vec{j} / \partial t . \quad (7)$$

This equation allows one to calculate the electric field $\vec{E}(\vec{r}, t)$ for given charge and current sources, $\rho(\vec{r}, t)$ and $\vec{j}(\vec{r}, t)$. Thus, equation (7) is the complete and correct formula for radiation. However, we want to apply it to a still simpler circumstance in which the second term (or, the current term) in the right-hand side of (7) provides the main contribution to the value of the radiation field. Since in the paraxial approximation the radiation field has only transverse components, we are interested in the transverse component of (7). Thus we consider the wave equation

$$c^2 \vec{\nabla}^2 \vec{E}_\perp - \partial^2 \vec{E}_\perp / \partial t^2 = 4\pi \partial \vec{j}_\perp / \partial t , \quad (8)$$

which relates the transverse component of the electric field to the transverse component of current density.

We wish to examine the case when the phase velocity of the current wave is close to the velocity of light. This requirement may be met under resonance condition

$$\omega/c = \omega/v_z - k_w . \quad (9)$$

First we may point out that the statement of (9), the condition for the relation between ω , k_w and v_z , is the condition for synchronism between the transverse electromagnetic wave and the

fast transverse current wave with the propagating constant $\omega/v_z - k_w$. With a current wave travelling with the same phase speed as the electromagnetic wave, we have a possibility of (space) resonance between electromagnetic wave and electrons. If this is the case, cumulative interaction between bunched electron beam and transverse electromagnetic wave takes place. We are therefore justified in considering the contributions of all the waves except the synchronous one to be negligible.

Any state of transverse electromagnetic wave can always be written as a linear combination of the two base states (polarizations). By given the amplitudes and phases of these base states we completely describe the electromagnetic wave state. It is usually best to start with the form which is physically clearest. We choose the Cartesian base states and seek the solution for \vec{E}_\perp in the form

$$E_{x,y} = \tilde{E}_{x,y}(z, \vec{r}_\perp) \exp[i\omega(z/c - t)] + \text{C.C.} \quad (10)$$

Here and in what follows, complex amplitudes related to the field are written with a tilde. The description of the field given by (10) is quite general. However, the usefulness of the concept of carrier wave number is limited to the case where the amplitude is slowly varying function of z .

To determine the form of $\tilde{E}_{x,y}(z, \vec{r}_\perp)$ we substitute (6) and (10) into (8), and have inside the undulator

$$\begin{aligned} & \exp[i\omega(z/c - t)] \left\{ \vec{\nabla}_\perp^2 + \frac{2i\omega}{c} \frac{\partial}{\partial z} + \frac{\partial^2}{\partial z^2} \right\} \begin{pmatrix} \tilde{E}_x \\ \tilde{E}_y \end{pmatrix} + \text{C.C.} \\ & = 4\pi \frac{\omega}{c} \begin{pmatrix} \cos(k_w z) \\ -\sin(k_w z) \end{pmatrix} e\theta_w a_{\text{in}} n_0(\vec{r}_\perp) \sin \omega(z/v_z - t). \end{aligned} \quad (11)$$

Here $\vec{\nabla}_\perp^2$ is the Laplace operator in transverse coordinates. At $z > L_w$ the right-hand side of (11) is equal to zero.

Now we have apparently simple pair of equations – and they are still exact. We simplify the equations by noting that for a radiation field it is reasonable to assume that $\tilde{E}_{x,y}$ are slowly varying function of z so that $\partial^2 \tilde{E}_{x,y} / \partial z^2$ may be neglected. The corresponding requirement for the complex amplitude is $|\partial \tilde{E}_{x,y} / \partial z| \ll k |\tilde{E}_{x,y}|$. In other words, the radiation pulse must not change significantly while travelling through a distance comparable with the wavelength $\lambda = 2\pi/k$. This assumption is not a restriction. Such is the case in all practical cases of interest. Differential equations becomes

$$\exp[i\omega(z/c - t)] \left\{ \vec{\nabla}_\perp^2 + \frac{2i\omega}{c} \frac{\partial}{\partial z} \right\} \begin{pmatrix} \tilde{E}_x \\ \tilde{E}_y \end{pmatrix} + \text{C.C.}$$

$$= 4\pi \frac{\omega}{c} \begin{pmatrix} \cos(k_w z) \\ -\sin(k_w z) \end{pmatrix} e^{\theta_w a_{in} n_0(\vec{r}_\perp)} \sin \omega(z/v_z - t). \quad (12)$$

Although equations (12) cannot be solved in general, we will solve them for some special cases. These equations can be simplified further by noting that the complex amplitudes $\tilde{E}_{x,y}$ will not vary much with z , especially in comparison with the oscillating terms $\exp(-i k_w z)$. The slow wave of transverse current oscillates very rapidly about an average value of zero and, therefore, does not contribute very much to the rate of change of $\tilde{E}_{x,y}$. So we can make a reasonably good approximation by replacing these terms by their average value, namely zero. We will leave them out, and take as our approximation:

$$\vec{\nabla}_\perp^2 \begin{pmatrix} \tilde{E}_x \\ \tilde{E}_y \end{pmatrix} + \frac{2i\omega}{c} \frac{\partial}{\partial z} \begin{pmatrix} \tilde{E}_x \\ \tilde{E}_y \end{pmatrix} = - \begin{pmatrix} i \\ 1 \end{pmatrix} 2\pi \frac{\omega}{c} e^{\theta_w a_{in} n_0(\vec{r}_\perp)} \exp(-i C z). \quad (13)$$

Even the remaining terms, with exponents proportional to $C = \omega/v_z - \omega/c - k_w$ will also vary rapidly unless C is near zero. Only then will the right-hand side vary slowly enough that any appreciable amount will accumulate when we integrate the equations with respect to z . The required conditions will be met if $C \ll k_w$, $1 \ll k_w z$. In other words, we use the resonance approximation here and assume that complex amplitudes $\tilde{E}_{x,y}$ are slowly varying in the longitudinal coordinate. By "slowly varying" we mean that $|\partial \tilde{E}_{x,y} / \partial z| \ll k_w |\tilde{E}_{x,y}|$. For this inequality to be satisfied, the spatial variation of $\tilde{E}_{x,y}$ within the undulator period $\lambda_w = 2\pi/k_w$ has to be small.

Equations (13) are simple enough and can be solved in any number of ways. One convenient way is the following. Taking the sum and the difference of the two we get

$$\left(\vec{\nabla}_\perp^2 + \frac{2i\omega}{c} \frac{\partial}{\partial z} \right) (\tilde{E}_x + i \tilde{E}_y) = 2\pi i \frac{\omega}{c} e^{\theta_w a_{in} n_0(\vec{r}_\perp)} \exp(-i C z), \quad (14)$$

$$\left(\vec{\nabla}_\perp^2 + \frac{2i\omega}{c} \frac{\partial}{\partial z} \right) (\tilde{E}_x - i \tilde{E}_y) = 0. \quad (15)$$

These equations describe the general case of electromagnetic wave radiation by the modulated electron beam in the helical undulator. Equations (14) and (15) refer to the right- and left-helicity components of the wave, respectively. The solutions for the right- and left-helicity waves are linearly independent. It follows from (14) and (15) that only those waves are radiated that have the same helicity as undulator field itself.

The electric field, \vec{E}_\perp , of the wave radiated in the helical undulator in resonance approximation is circularly polarized and may be represent in the complex form:

$$E_x + i E_y = \tilde{E}(z, \vec{r}_\perp) \exp[i\omega(z/c - t)].$$

Finally, the equation for \tilde{E} can be written in the form

$$\left(\nabla_{\perp}^2 + \frac{2i\omega}{c} \frac{\partial}{\partial z} \right) \tilde{E} = 2\pi i \frac{\omega}{c} e\theta_w a_{\text{in}} n_0(\vec{r}_{\perp}) \exp(-iCz). \quad (16)$$

Equation (16) is an inhomogeneous parabolic equation. Its solution can be expressed in terms of a convolution of the free-space Green's function (impulse response)

$$G(z - z', \vec{r}_{\perp} - \vec{r}'_{\perp}) = \frac{1}{4\pi(z - z')} \exp \left[\frac{i\omega}{2c(z - z')} |\vec{r}_{\perp} - \vec{r}'_{\perp}|^2 \right]$$

with the source term. When the right-hand side of (16) is equal to zero, it transforms to the well-known paraxial wave equation in optics.

The radiation process displays resonance behavior, and the amplitude of electric field depends strongly on the value of the detuning parameter C . With the approximation made in getting (16) the equation can be solved exactly. Now we will find an exact solution for the case of perfect resonance. When the parameters are tuned to perfect resonance, such that $C = 0$, the solution of the equation (16) has the form

$$\tilde{E}(z, \vec{r}_{\perp}) = \frac{ie\theta_w \omega a_{\text{in}}}{2c} \int_0^z \frac{dz'}{z - z'} \int d\vec{r}'_{\perp} n_0(\vec{r}'_{\perp}) \exp \left[\frac{i\omega}{2c(z - z')} |\vec{r}_{\perp} - \vec{r}'_{\perp}|^2 \right], \quad (17)$$

where (z, \vec{r}_{\perp}) and (z', \vec{r}'_{\perp}) are the coordinates of the observation and the source point, respectively.

Let us consider an axisymmetric electron beam with gradient profile of the current density. In this case we have $-ev_z n_0(\vec{r}_{\perp}) = -j_0 S(r)$, where r is the radial coordinate of the cylindrical system (r, ϕ, z) and $S(r)$ describes the transverse profile of the electron beam. To be specific, we write down all the expressions for the case of a Gaussian transverse distribution:

$$-ev_z n_0(\vec{r}_{\perp}) = -\frac{I_0}{2\pi\sigma^2} \exp \left(-\frac{r^2}{2\sigma^2} \right),$$

where I_0 is the total beam current. Then we can write (17) in the form

$$\begin{aligned} \tilde{E}(z, r) &= \frac{ie\theta_w \omega a_{\text{in}} I_0}{2c} \int_0^z \frac{dz'}{z - z'} \int_0^{\infty} dr' r' \exp \left[-\frac{(r')^2}{2\sigma^2} \right] \\ &\times J_0 \left(\frac{\omega r' r}{z - z'} \right) \exp \left[\frac{i\omega(r')^2 + i\omega r^2}{2c(z - z')} \right]. \end{aligned} \quad (18)$$

It is convenient to rewrite this expression in a dimensionless form. After an appropriate normalization it is a function of one dimensionless parameter only:

$$\begin{aligned} \hat{E} &= f(\hat{z}, \hat{r}, N) = \frac{i}{N} \int_0^{\hat{z}} \frac{d\hat{z}'}{\hat{z} - \hat{z}'} \int_0^\infty d\hat{r}' \hat{r}' \exp \left[-\frac{(\hat{r}')^2}{2N} \right] \\ &\times J_0 \left(\frac{\hat{r}' \hat{r}}{\hat{z} - \hat{z}'} \right) \exp \left[\frac{i(\hat{r}')^2 + i\hat{r}^2}{2(\hat{z} - \hat{z}')} \right]. \end{aligned} \quad (19)$$

where $\hat{z} = z/L_w$, $\hat{r} = \sqrt{kr^2/L_w}$, $k = \omega/c$, L_w is the total undulator length, $N = k\sigma^2/L_w$ is the diffraction parameter (or, Fresnel number of the electron beam), $\hat{E} = \tilde{E}/E_0$ is the normalized field amplitude, and

$$E_0 = \frac{\theta_w \omega a_{in} I_0}{2c^2}.$$

Integrating first with respect to \hat{r}' , we have

$$\hat{E} = i \int_0^{\hat{z}} \frac{d\hat{z}'}{\hat{z} - \hat{z}' + iN} \exp \left[-\frac{i\hat{r}^2}{2(\hat{z} - \hat{z}' + iN)} \right]. \quad (20)$$

The integration over source coordinate \hat{z}' can be performed without great difficulty in limiting case, namely, the case of diffraction parameter very large compared with unity. In this case the integral in (20) is calculated analytically

$$\hat{E} = \frac{\hat{z}}{N} \exp \left(-\frac{\hat{r}^2}{2N} \right) \quad \text{as } N \gg 1.$$

It is convenient to express electric field inside the wide electron beam in dimension form

$$\tilde{E}(z, \vec{r}_\perp) = \pi e \theta_w z a_{in} n_0(\vec{r}_\perp) = \frac{\theta_w z a_{in} I_0}{2c\sigma^2} \exp \left(-\frac{r^2}{2\sigma^2} \right) \quad \text{as } N \gg 1. \quad (21)$$

Note that this result is completely general: that is, it applies for any electron beam profile. To calculate equation (17) we note that the behavior of Green's function for $k\sigma^2 \gg L_w$ approaches the behavior of the delta function. The source function $n_0(\vec{r}'_\perp)$ does not vary very much across the region $|\vec{r}_\perp - \vec{r}'_\perp|^2 \simeq L_w/k$ in the case of wide electron beam: therefore we can replace it by a constant. In other words, we simply take $n_0(\vec{r}'_\perp)$ outside the integral sign and call it $n_0(\vec{r}_\perp)$.

The radiation field distribution at the exit of undulator is one of the important characteristics of the radiator. For the case of Gaussian electron beam profile transverse profile of the radiation field is presented in Fig. 13. Since the slow varying field amplitude $\hat{E}(\hat{z}, \hat{r})$ is given by complex function of the transverse coordinate, the wavefront of output radiation is not plane. It is interesting to trace the variation of the field phase across the radiation beam. Bottom plot in Fig. 13 shows the distribution of the phase of the radiation beam for several values of the diffraction parameter N .

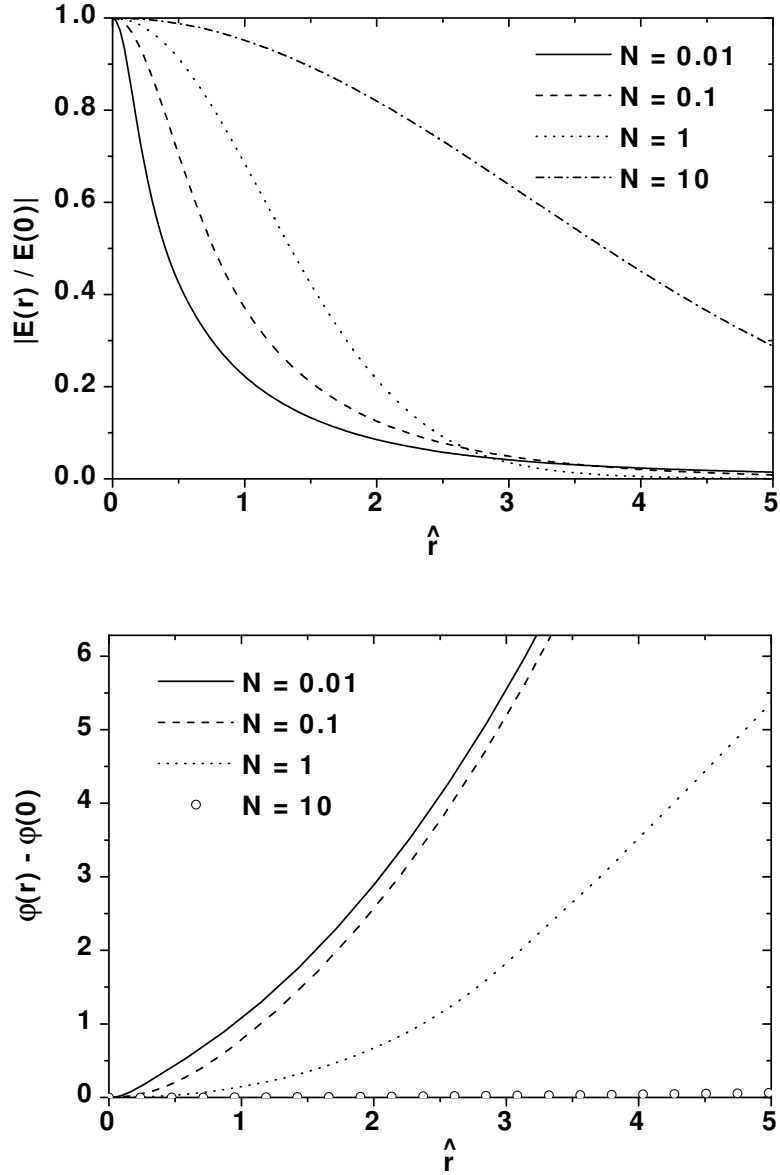


Fig. 13. Electron beam with Gaussian profile: transverse distribution of the field amplitude (top) and phase (bottom) at the radiator undulator exit for several values of the diffraction parameter N from 0.01 to 10. Here detuning parameter $C = 0$

It is interesting to plot the normalized amplitude of electric field as a function of diffraction parameter in order to see how sensitive it is to electron beam size. At this point we find it convenient to impose the following restriction: we focus only on the radiation seen by observer lying on the electron beam axis. We show such a plot in Fig. 14. When $\hat{r} = 0$ we can write (20)

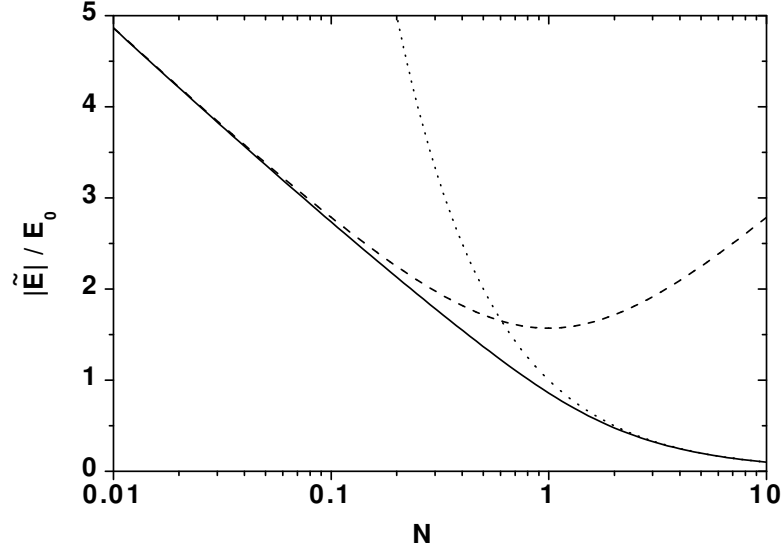


Fig. 14. Electron beam with Gaussian profile. The reduced radiation field amplitude versus the diffraction parameter at $\hat{z} = 1, \hat{r} = 0$. Here detuning parameter $C = 0$. Dashed line shows asymptote of thin electron beam. Dotted line shows asymptote of wide electron beam

in the form

$$\hat{E} = f(\hat{z}, 0, N) = i \int_0^{\hat{z}} \frac{d\hat{z}'}{\hat{z} - \hat{z}' + iN} = \arctan\left(\frac{\hat{z}}{N}\right) + \frac{i}{2} \ln\left(1 + \frac{\hat{z}^2}{N^2}\right).$$

Let us study the asymptotic behavior of the field amplitude at the large values of the diffraction parameter N . In this case $\hat{z}/N \ll 1$ and we have asymptotically:

$$\hat{E} = f(\hat{z}, 0, N) \rightarrow \hat{z}/N \quad \text{as } N \rightarrow \infty.$$

Now let us study the asymptote of a thin electron beam. In this case $N \rightarrow 0$ and the function $f(\hat{z}, 0, N)$ can be estimated simply as:

$$\hat{E} = f(\hat{z}, 0, N) \rightarrow \pi/2 + i \ln(\hat{z}/N) \quad \text{as } N \rightarrow 0. \quad (22)$$

Special attention is called to the fact that in the thin beam case, at $N \rightarrow 0$, amplitude \tilde{E} is a complex function. One immediately recognizes the physical meaning of the complex \tilde{E} . Note that electric field (response) is given by the fast wave of transverse current ("force") times a certain factor. This factor can either be written as $p + iq$, or as certain magnitude ρ times $\exp(i\delta)$. If it is written as a certain amplitude ρ times $\exp(i\delta)$, let us see what it means. This tells us that electric field is not oscillating in phase with the fast wave of transverse current,

which has (at $C = 0$) the phase $\psi = \omega z/c - \omega t$, but is shifted by an extra amount δ . Therefore $\delta(z)$ represent the phase shift of the response. For the experts in FEL physics we should add that logarithmic terms in (22) and logarithmic growth rate asymptote for conventional FEL amplifier at small diffraction parameter (see [17]) are ultimately connected.

From practical point of view it is necessary to know the field distribution in the space after the undulator, at $z > L_w$. When the radiation field leaves the undulator, it is subjected to the parabolic equation

$$\left(\vec{\nabla}_{\perp}^2 + \frac{2i\omega}{c} \frac{\partial}{\partial z} \right) \tilde{E} = 0.$$

It follows from the latter equation that the field amplitude in the space after the undulator and the field amplitude at the undulator exit are connected by

$$\tilde{E}(z, \vec{r}_{\perp}) = \frac{1}{4\pi(z - L_w)} \int d\vec{r}'_{\perp} \tilde{E}(L_w, \vec{r}'_{\perp}) \exp \left[\frac{i\omega}{2c(z - L_w)} |\vec{r}_{\perp} - \vec{r}'_{\perp}|^2 \right].$$

The subject of particular interest is the angular distribution of the radiation intensity. The radiation field at the undulator exit may be presented as a superposition of plane waves, all with the same wave number $k = \omega/c$. The value of k_{\perp}/k gives the sine of the angle between the z axis and the direction of propagation of the plane wave (we consider the axisymmetric case). In the paraxial approximation $k_{\perp}/k = \sin \theta \simeq \theta$. The angular distribution of the radiation intensity, $I(\theta)$, can be expressed as follows:

$$\frac{I(\theta)}{I(0)} = \frac{|\Xi(\theta)|^2}{|\Xi(0)|^2},$$

where $\Xi(\theta)$ is the spatial Fourier transform of the complex amplitude of the radiation field, $\tilde{E}(z, r)$ at the exit of the undulator. In the axisymmetric case the spatial Fourier transform of the radiation field is given by

$$\Xi(\hat{\theta}, N) = \int_0^{\infty} \hat{E}(1, \hat{r}, N) J_0(\hat{\theta} \hat{r}) \hat{r} d\hat{r},$$

where $\hat{\theta} = \sqrt{kL_w} \theta$ and J_0 is the Bessel function of the first kind. Using (20), we find the expression for the angular distribution of the radiation intensity,

$$\frac{I(\theta)}{I(0)} = \frac{|\Xi(\theta)|^2}{|\Xi(0)|^2} = \left[\frac{\sin \hat{\theta}^2/4}{\hat{\theta}^2/4} \right]^2 \exp(-N\hat{\theta}^2).$$

At large value of diffraction parameter N the far zone approximation may be used when $z_0/(k\sigma^2) \gg 1$, where z_0 is the distance between the observation point and the undulator exit. When $N < 1$

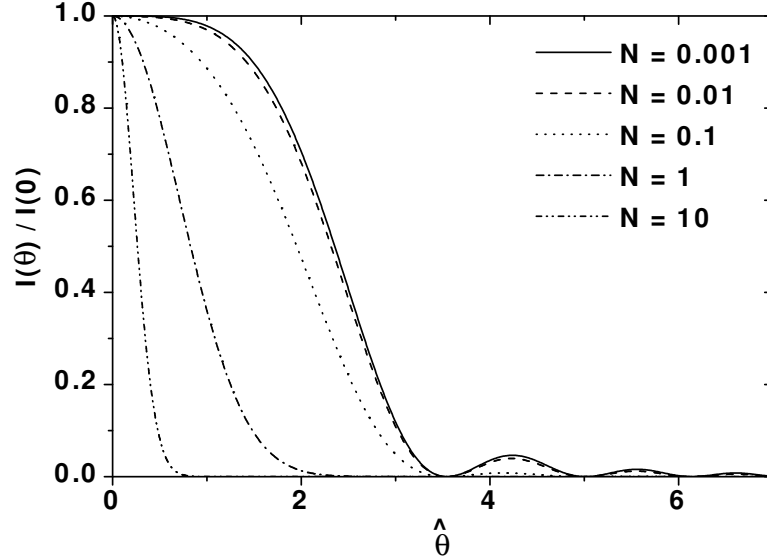


Fig. 15. Electron beam with Gaussian profile. Angular distribution of the radiation intensity for several values of the diffraction parameter N from 0.001 to 10. Here detuning parameter $C = 0$

the above condition changes to $z_0 \gg L_w$. Figure 15 presents the angular distribution of the radiation intensity for the coherent undulator radiation in the case of Gaussian profile of electron beam. One can see that the radiation power is mainly concentrated in the small angle near the z axis. At large value of the diffraction parameter the distribution is approximately equal to

$$\frac{|\Xi(\hat{\theta})|^2}{|\Xi(0)|^2} \rightarrow \exp(-N\hat{\theta}^2) \quad \text{as } N \rightarrow \infty .$$

In the case of a thin electron beam we have asymptotically:

$$\frac{|\Xi(\hat{\theta})|^2}{|\Xi(0)|^2} \rightarrow \left[\frac{\sin \hat{\theta}^2/4}{\hat{\theta}^2/4} \right]^2 \quad \text{as } N \rightarrow 0 .$$

Let us investigate qualitatively the process of coherent undulator radiation. To get an intuitive picture on what happens with the radiation beam let us first choose a thin beam asymptotic. This is an example in which diffraction effects play an important role. Simple physical consideration can lead directly to a crude approximation for the radiation beam cross-section. There is a complete analogy between the radiation effects of the bunched electron beam in the undulator and the radiation effects of a sequence of periodically spaced oscillators. The radiation of these oscillators always interferes coherently at zero angle with respect to the undulator axis. When all the oscillators are in phase there is a strong intensity in the direction $\theta = 0$. An interesting question is, where is the minimum? If we have a triangle with a small altitude $r \simeq z\theta$ and a long base

z , then the diagonal s is longer than the base. The difference is $\Delta = s - z \simeq r^2/2z \simeq z\theta^2/2$. When Δ is equal to one wavelength, we get a minimum because the contributions of various oscillators are then uniformly distributed in phase from 0 to 2π . In the limit of small size of the electron beam interference will be constructive within an angle of about $\theta_c \simeq (\sqrt{kz})^{-1}$. In the limit of large electron beam size, the field is concentrated mainly inside the electron beam. The radiation field across the electron beam may be present as a superposition of plane waves. We can expect that the typical width of the angular spectrum should be of the order $\theta_c \simeq (k\sigma)^{-1}$, simply a consequence of the reciprocal width relations of the Fourier transform pair $\Delta k_{\perp} \sigma \simeq 1$.

The boundary between these two asymptotes is about $k\sigma \simeq \sqrt{kL_w}$ or (another way to write it) $\sigma^2 \simeq \sigma_{\text{dif}}^2 = L_w/k$. A rough estimate for the diffraction effects to be small is $\sigma \gg L_w/(k\sigma)$, which simply means that the diffraction expansion of the radiation at undulator length must be much less than the size of the beam. Another way to write this condition is $k\sigma^2/L_w = N \gg 1$. As we mentioned above, the diffraction parameter N can be referred to as the electron beam Fresnel number.

Let us consider the electromagnetic power. The well-known Poynting vector represents the electromagnetic power flow. In the paraxial approximation the diffraction angles are small, the vectors of electric and magnetic field are equal in absolute value and are perpendicular to each other. Thus, the expression for the radiation power, W , can be written in the form:

$$W = \frac{c}{4\pi} \int \overline{|\vec{E}_{\perp}|^2} d\vec{r}_{\perp} = \frac{c}{4\pi} \int |\tilde{E}(z, \vec{r}_{\perp})|^2 d\vec{r}_{\perp}, \quad (23)$$

where $\overline{(\dots)}$ denotes averaging over a cycle of oscillation of the carrier wave. If we consider a system with fields and bunched electron beam in an undulator, the energy stored in any volume fluctuates sinusoidally with time. But on the average there is no increase or decrease in the energy stored in any portion of the volume.

Now we shall calculate the output power. To determine the W we substitute (18) into (23). It is convenient to write the expression for W in a dimensionless form. After an appropriate normalization it is a function of one dimensionless parameter only:

$$\hat{W} = F(N), \quad (24)$$

where $N = k\sigma^2/L_w$ is the diffraction parameter, $\hat{W} = W/W_0$ is the normalized power, and W_0 is

$$W_0 = \frac{\pi\theta_w^2\omega I_0^2 a_{\text{in}}^2 L_w}{8c^2}.$$

Substituting the expression for \tilde{E} from (20) into (23), we obtain:

$$F(N) = \frac{2}{\pi} \left[\arctan \left(\frac{1}{2N} \right) + N \ln \left(\frac{4N^2}{4N^2 + 1} \right) \right]. \quad (25)$$

In Fig. 16 we present a plot of this universal function. The physical implication of this result are best understood by considering some limiting cases. We have asymptotically:

$$F(N) \rightarrow 1/(2\pi N) \quad \text{as} \quad N \rightarrow \infty ,$$

$$F(N) \rightarrow 1 \quad \text{as} \quad N \rightarrow 0 ,$$

Let us notice a remarkable feature of that plot. In the limit of a thin electron beam, $N \rightarrow 0$, the radiation power tends to a constant value $W \rightarrow W_0$ and the dependence of output radiation on the transverse size of the electron beam is rather weak.

For practical purposes it is convenient to express W_0 in an explicit form:

$$W_0 = W_b \left[\frac{\pi^2 a_{\text{in}}^2}{2} \right] \left[\frac{I}{\gamma I_A} \right] \left[\frac{K^2}{1 + K^2} \right] N_w , \quad (26)$$

where $W_b = m_e c^2 \gamma I_0 / e$ is the total power of electron beam, $I_A = m_e c^3 / e \simeq 17$ kA is the Alfvén current. Let us make a calculation of W for some cases. Suppose $a_{\text{in}} = 0.3$, $I_0 = 3$ kA, $\gamma = 10^3$, $K = 5.4$, $N_w = 5$; then by equation (26) it follows that $W_0 \simeq 500$ MW. If the laser wavelength $\lambda = 1 \mu\text{m}$, the normalized transverse emittance $\epsilon_n = 2\pi \mu\text{m}$, focusing beta function is equal to 1 m, the diffraction parameter is about 0.04. Remembering the previous result (see Fig. 16) we come to the conclusion that we can treat this situation as a coherent undulator radiation with thin electron beam.

It is relevant to make some remarks on the region of applicability of the results of this section. One of the basic assumptions of the theory is that the radius of the electron rotation in the undulator, $r_w = \theta_w / k_w$, is much less than the transverse size of the electron beam. Taking into account that $\theta_w = K/\gamma$, we can write

$$\frac{\sigma^2}{r_w^2} = \frac{1 + K^2}{K^2} \left(\gamma_z^2 \sigma^2 k_w^2 \right) = \frac{1 + K^2}{K^2} (\pi N_w N) \gg 1 .$$

Thus, the requirement for the parameter σ^2/r_w^2 to be large can be written as $\pi N_w N \gg 1$. When the diffraction parameter N is much larger than $(\pi N_w)^{-1}$, the radius of the electron rotation in the undulator is always much less than the transverse size of the electron beam. In our example we have $N \simeq (\pi N_w)^{-1}$. We should say that this particular case is at the boundary of the region of the applicability of our theory.

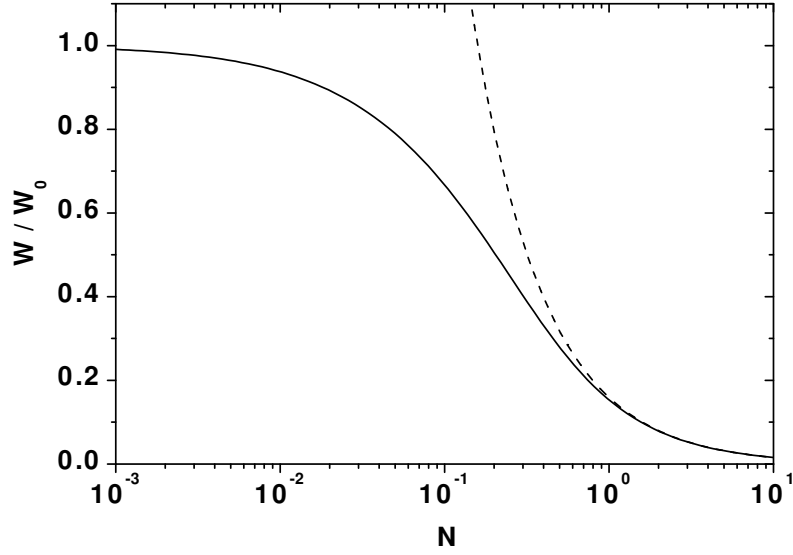


Fig. 16. Electron beam with Gaussian profile. The reduced output power versus the diffraction parameter. Solid curve is calculated with analytical formula (25). Dashed curve shows an asymptote for a wide electron beam. Here the detuning parameter is $C = 0$

The formula for the output power which we derived (24) refer to the case of the helical undulator. It can be simply generalized for the case of a planar undulator. The magnetic field on the axis of the planar undulator is given by

$$\vec{H} = \vec{e}_x H_w \cos(k_w z) .$$

The explicit expression for the electron velocity in the field of the planar undulator has the form:

$$\vec{v}_\perp = -\vec{e}_y c \theta_w \sin(k_w z) ,$$

where $\theta_w = K/\gamma = \lambda_w e H_w / (2\pi m_e c^2 \gamma)$. The constrained motion of the electron in the planar undulator differs from that in the helical one. An important feature of this motion is that longitudinal velocity v_z of the electron oscillates along the undulator axis which creates definite problems for the description of the radiation process. It is not hard to go through the derivation of radiation power again. If we do that, and calculate the power in the same way, we get that all the expressions for the planar undulator are identical to those for the helical undulator. The only difference is the appearance of different numerical factors taking their origin from the averaging procedure. One can obtain that expression for power written down in the reduced form is identical for both undulator configurations. As a result, the universal plot $\hat{W} = F(N)$ in Fig. 16 is applicable to the case of planar undulator, too. The only difference is that the following

definition of normalization factor for the radiator with planar undulator should be used:

$$W_0 = \frac{\pi \theta_w^2 A_{JJ}^2 \omega_0 I_0^2 a_{in}^2 L_w}{16c^2},$$

where

$$A_{JJ} = [J_0(Q) - J_1(Q)],$$

$J_n(Q)$ is a Bessel function of n th order, and

$$Q = \theta_w^2 \omega_0 / (8k_w \gamma^2) = K^2 / (4 + 2K^2).$$

When we simplified the expression for Q , we used the resonance condition for the planar undulator $\omega_0 = 2\gamma^2 k_w / [c(1 + K^2/2)]$. For practical purposes it is convenient to rewrite the expression for W_0 in the form

$$W_0 = W_b \left[\frac{\pi^2 a_{in}^2}{2} \right] \left[\frac{I}{\gamma I_A} \right] \left[\frac{K^2}{2 + K^2} \right] A_{JJ}^2 N_w.$$

Let us present a specific numerical example for the case of a radiator with a planar undulator. With the numerical values $\lambda_w = 6.5$ cm, $K = 7.6$, $\gamma = 10^3$, the resonance value of wavelength is $\lambda = 1\mu\text{m}$. If the number of the undulator periods $N_w = 5$, the amplitude of density modulation $a_{in} = 0.3$, the beam peak current $I_0 = 3$ kA, the radiation power is about $W = W_0 F(N) \simeq 250 F(N)$ MW.

All of the foregoing discussion of coherent undulator radiation has been concerned solely for the radiation at resonance – that is $\omega = \omega_0 = 4\pi\gamma_z^2 c / \lambda_w$. Now, we would like to find out how the output radiation varies in the circumstance that seed signal frequency ω is nearly, but not exactly, equal to ω_0 . According to the radiation equation (16), the radiation process is determined by the detuning $C = k_w + \omega/c - \omega/v_z$ which is the function of the seed laser frequency, energy of the electron beam and the undulator parameter. It is not hard to go through the derivation of output radiation power again. If we take $C \neq 0$, the solution of the wave equation (16) has the form

$$\begin{aligned} \tilde{E}(z, \vec{r}_\perp) &= \frac{i e \theta_w \omega a_{in}}{2c} \int_0^z \frac{dz'}{z - z'} \exp(-i C z') \\ &\times \int d\vec{r}'_\perp n_0(\vec{r}'_\perp) \exp \left[\frac{i \omega |\vec{r}_\perp - \vec{r}'_\perp|^2}{2c(z - z')} \right]. \end{aligned} \quad (27)$$

When the electron beam profile is Gaussian, we can write (27) in a dimensionless form:

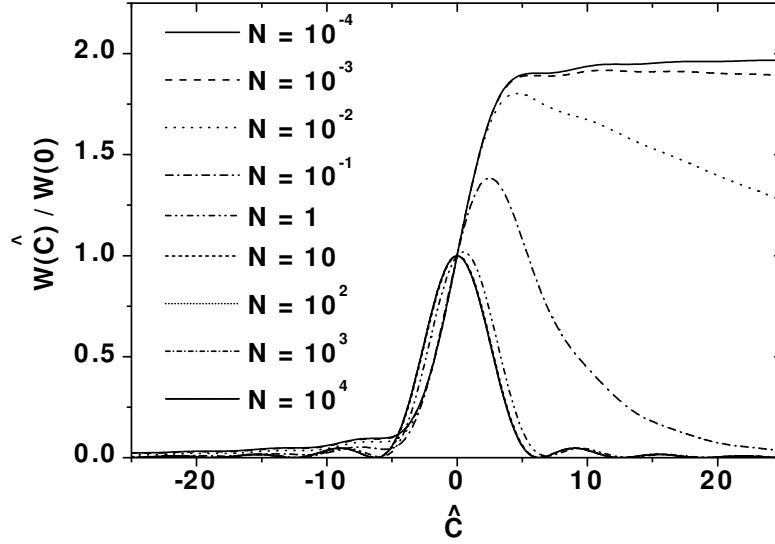


Fig. 17. Electron beam with Gaussian profile. The reduced output power versus the reduced detuning \hat{C} for various values of Fresnel number

$$\begin{aligned}
\hat{E} &= f(\hat{z}, \hat{r}, N, \hat{C}) = \frac{i}{N} \int_0^{\hat{z}} \frac{d\hat{z}'}{\hat{z} - \hat{z}'} \int_0^{\infty} d\hat{r}' \hat{r}' \exp\left[-\frac{(\hat{r}')^2}{2N}\right] \exp(-i\hat{C}\hat{z}') \\
&\times J_0\left(\frac{\hat{r}'\hat{r}}{\hat{z} - \hat{z}'}\right) \exp\left[\frac{i(\hat{r}')^2 + i\hat{r}^2}{2(\hat{z} - \hat{z}')}\right] = i \int_0^{\hat{z}} \frac{d\hat{z}'}{\hat{z} - \hat{z}' + iN} \\
&\times \exp\left[-\frac{i\hat{r}^2}{2(\hat{z} - \hat{z}' + iN)}\right] \exp(-i\hat{C}\hat{z}'). \quad (28)
\end{aligned}$$

We use the notations similar to those introduced above. Also, an additional parameter of the problem, the dimensionless detuning parameter $\hat{C} = CL_w$, appears in the theory, since we take into account resonance behavior. Let us express \hat{C} in terms of physical parameters. The detuning parameter \hat{C} is connected by the simple relation with the frequency deviation: $\omega - \omega_0 = \Delta\omega = -2\gamma_z^2 C$. Thus, we obtain $\hat{C} = -2\pi N_w \Delta\omega / \omega_0$, where N_w is the number of radiator undulator periods.

Let us now study the influence of the detuning on the radiation process. In Fig. 17 the output power is shown as a function of reduced detuning for different values of diffraction parameter. One can see that the radiation process displays resonance behavior and the output power depends strongly on the value of the detuning parameter \hat{C} . It is seen from the plot that at large value of Fresnel number the resonance curve is simply that of the interference factor,

$$f(\hat{C}) = \frac{\sin^2(\hat{C}/2)}{(\hat{C}/2)^2}.$$

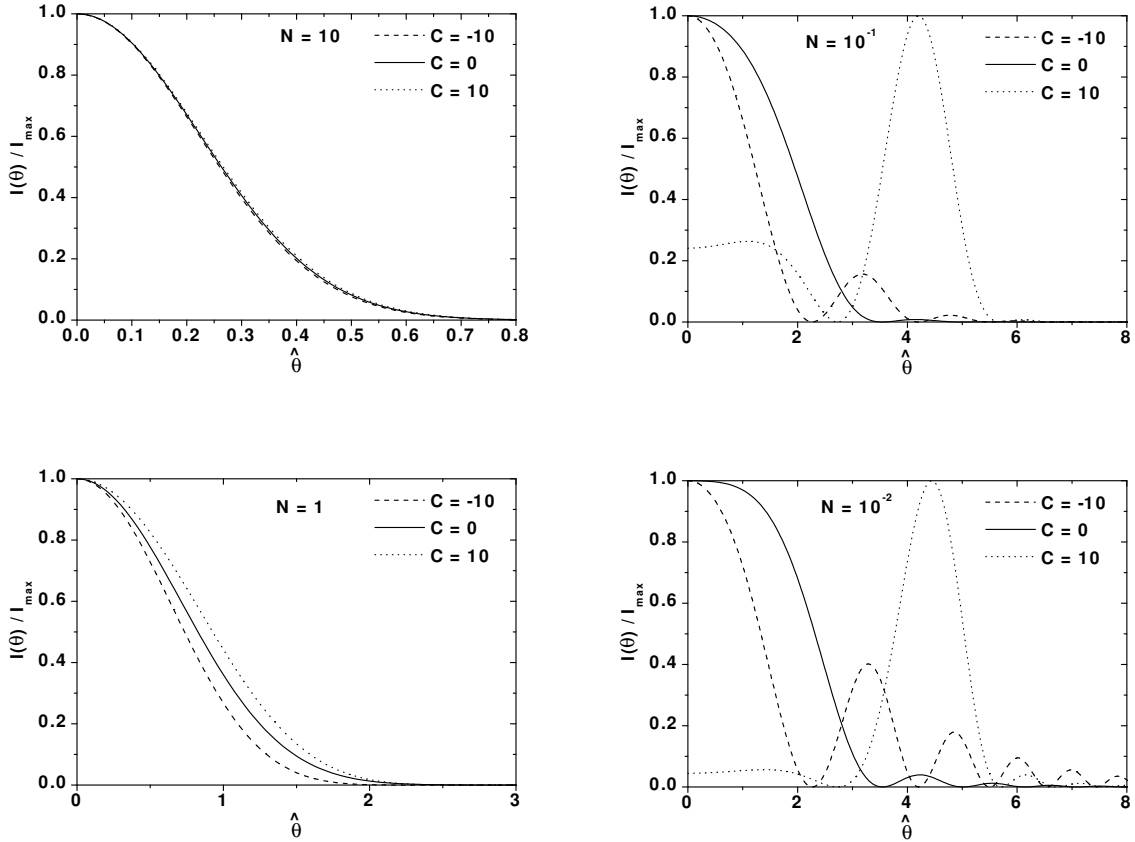


Fig. 18. Electron beam with Gaussian profile. Angular distribution of the radiation intensity for several values of the diffraction parameter. Curves correspond to the detuning parameter $\hat{C} = -10, 0, \text{ and } 10$

One can see that this formula works well at $N \simeq 10$. Then, at $N \simeq 1$, the resonance curve is visibly modified due to diffraction effects. One can see from this plot that the resonance curve is not completely symmetrical function of the detuning parameter \hat{C} , the asymmetry being greater for smaller Fresnel number. The reason for this is that at small values of diffraction parameter the angular distribution of the radiation corresponds to that emitted by a simple one electron. To explain this phenomena, we should analyze the angular distribution of the radiation intensity. Even without performing calculations, we can expect angular-frequency dependence for the output radiation in the case of a thin electron beam asymptote. As we can see from Fig. 18, numerical calculations in the far zone confirm this simple physical consideration.

5 Discussion

Successful operation of the ultrashort-pulse-measurement device (FROG) requires the fulfillment of several requirements. The requirement for the spatio-temporal pulse distortions to be small is of importance for the performance of the FROG measurement apparatus. One of

the problems is the measurement of the pulses that have significant spatial structure, for example, a pulse whose transverse size varies along the pulse. For the FROG is of great interest to minimize ultrafast variation of the optical replica transverse size which is due to emittance variation along the electron bunch. Obviously, this requirement is easier to achieve for a thin electron beam asymptote. On the other hand, such ultrafast variation of the pulse transverse size is an essential characteristic of the optical replica in a wide electron beam case, since it reflects behavior of a slice emittance. The obvious solution of this problem is as follows. A technique best suited for the pulses with spatial structure consists of expanding the radiation beam and filtering out the central part to almost constant transverse size. A spatial filter can be realized by using optical arrangement where a telescope is placed between replica synthesizer exit and FROG device. The pulse to be measured is propagated through the hole which spatially filters the pulse. The important point is that electric field of such filtered pulse contains completely the same information about transverse size of the electron bunch as initial pulse. If the electron beam is wide, $N \gg 1$, then electric field of the filtered replica is inversely proportional to the square of electron beam $E(t) \simeq \text{const.} \times I(t)/\sigma^2(t)$.

One of the big unsolved problems of the electron bunch diagnostics is measurement of bunches that have significant distortions in transverse phase space, for example, a bunch whose transverse phase space ellipse varies from point to point in the beam. We have considered in section 2 a simplified model of the electron beam and used the following assumptions: i) the electron beam transverse profile is assumed to be axisymmetric; ii) Twiss parameters are equal in all slices (although emittances are different). Such a beam can, in principle, be realized in an "idealized" RF photoinjector with a perfectly working emittance compensation technique [18] that allows one to align slices in transverse phase space. For real beam, the variation in the space charge forces can be significant and cannot be properly compensated with solenoidal emittance compensation that was observed in different measurements [19–21]. In addition, CSR-related effects in bunch compressors can lead to further deviations from the simple model. It is clear that a knowledge of the variation of phase space ellipse along the bunches at the output of the bunch formation system could provide significant information about the physical mechanisms responsible for generation of ultrashort bunches. Here we would like to discuss a further extension of the proposed diagnostic method that can allow one to determine Twiss parameters in axial slices that are only a μm -long fraction of the full bunch length.

A very simple approach, involving simultaneous "quadrupole-scan" and "hole-scan" techniques, yields the solution. The main idea can easily be understood taking into account the fact that in the limit of a wide electron beam we measure the beam size, and therefore, we can, in principle, use a standard "quadrupole-scan" technique. Moreover, the method of spatial filtering described above allows one to determine a transverse distribution of the beam density

in each slice. Indeed, in the limit of a wide beam the electric field at the undulator exit (21) is directly proportional to the beam density distribution (this holds also for non-axisymmetric beam when both sizes, in x - and y -directions, are much larger than a diffraction size). FROG technique and spatial filter allow the two-dimensional slice density distribution measurements to be made using a "hole-scan" technique. Therefore, one can do a quadrupole scan (using a system of quadrupoles) by changing phase advance but keeping all slices in a wide beam limit. For each settings of the quadrupoles one does two-dimensional scan with a filter, checking that slice sizes are in the limit of wide beam. Then emittances and Twiss parameters in each slice are reconstructed by the standard method. If there are offsets and angles of slice centroids (due to CSR effects, for example), they can also be reconstructed from this measurement. Note also that after two-dimensional scan of the hole one gets three-dimensional map of the electric field amplitude that is a copy of three-dimensional density distribution in the electron bunch. Since total charge is known, the unknown absolute value of the current density can be determined, too. This approach appropriately can be referred to as bunch phase space tomography.

The main emphasis of previous considerations was concentrated on the measurements of ultrashort (sub-100 fs long) electron bunches. The method proposed can be also applied for measurements of long (a few ps) bunches, too. Measurements of such bunches is practically important problem. The X-ray FEL bunch compressors consist of a series of magnetic chicanes. To setup the compression, the bunch structure needs to be measured before and after each compression stage. In addition, once the bunch compressors are set up, a bunch length feedback system will be required for stabilization of the compression. The electron pulse durations of interest are approximately 10, 2 and 0.2 ps, respectively. The big advantage of the proposed diagnostic technique is the absence of apparent limitations which would prevent determination of the structure of electron bunches even without bunch compression in the injector linac. According to our discussion above, the pulse energy of optical replica is proportional to the value of the peak current which is relatively weak dependence. The energy of radiated pulse is about $10\mu\text{J}$ for the case when $I = 3\text{ kA}$. The energy per pulse is decreased by only a factor 30, down to sub- μJ level for $I = 100\text{ A}$. FROG technique still works well for such parameters of optical pulse. It has been used to measure pulses from a few fs to many ps in length. It has measured pulses from pJ to mJ in energy. FROG has proven to be a general technique that works [9].

Operation of the proposed scheme was illustrated for the parameters of the European XFEL. Although the present work is illustrated for the electron beam energy of 0.5 GeV, its applicability is not restricted to this range. For example, LCLS bunch compressor system [5] is a suitable candidate for application of diagnostic techniques described here.

6 Conclusion

Sub-100 fs ultrarelativistic electron bunches, which only a few years ago seemed like wishful thinking, are now effectively generated in the accelerator test facilities and have given a rise to ultrafast X-ray applications. The femtosecond time scale is beyond the range of standard electronic display instrumentation, and the development of the methods for the measurement of the longitudinal beam current distribution in such short bunches is undoubtedly a challenging problem. In this paper we proposed a new method for ultrashort electron pulse-shape measurements. Making the use of the ultrashort laser pulse-shape measurement device (FROG) together with carefully designed undulator-based optical replica synthesizer allow the electron bunch length measurement with resolution of about a few femtosecond. We demonstrate that proposed measuring device can be used to determine the electron current profile for a single ultrashort electron bunch, which makes it an ideal online tool for optimization of complex bunch compression systems. In general case the electron bunches may have significant emittance and energy spread variation along the bunch. Proposed device is capable to measure both of these electron bunch distortions quantitatively, too. An important feature of the method is that all steps of the optical replica synthesis are controlled by means of the choice of the undulator parameters, dispersion section strength and value of beta function. Data sets of beta function and dispersion section strength scans actually contain all the required information for retrieval of the slice properties of the bunch. Thus, proposed technique combines full-information electron bunch measurement with much-needed experimental simplicity. The only requirement for the proposed technique is the capability of the electron bunch to generate $1\mu\text{m}$ radiation, which implies a minimum on the electron energy of about one hundred MeV. However, this limit nicely fits in the design parameters of bunch compression systems for XFELs. Another key element – laser pulse-shape measurement device (FROG) – is now a standard and well-developed tool. All key elements of measuring device have already been established. Operating range of proposed diagnostic technique nicely includes that of most ultrashort X-ray FEL injector linacs, so it should be ideal for most everyday diagnostics as well as many more exotic ones.

Acknowledgments

We thank G. Geloni for many useful discussions. We thank R. Brinkmann, J.R. Schneider, A. Schwarz, and D. Trines for interest in this work.

References

- [1] V. Ayvazyan et al., Phys. Rev. Lett. 88(2002)104802.
- [2] V. Ayvazyan et al., Eur. Phys. J. D20(2002)149.
- [3] TESLA Technical Design Report, DESY2001-011, edited by Richard et al., and <http://tesla.desy.de>.
- [4] P. Audebert et al., "TESLA XFEL: First stage of the X-ray laser laboratory – Technical design report (R. Brinkmann et al., Eds.)", Preprint DESY 2002-167.
- [5] The LCLS Design Study Group, LCLS Design Study Report, SLAC reports SLAC-R-593 (2002) and <http://www-ssrl.slac.stanford.edu/lcls/CDR>.
- [6] M. Borland et al., Nucl. Instrum. and Methods A483(202)268.
- [7] M. Dohlus et al., "Start-to-End Simulations of SASE FEL at the TESLA Test Facility, Phase 1" Preprint DESY 03-197, DESY, Humburg, 2003; Nucl. Instrum. and Methods (in press).
- [8] P. Emma et al., Phys. Rev. Lett. 92(2004)074801.
- [9] R. Trebino, Frequency-Resolved Optical Gating: Measurement of Ultrashort Laser Pulses, Kluwer Academic Publishers, Boston, 2002.
- [10] E.L. Saldin, E.A. Schneidmiller and M.V. Yurkov, Nucl. Instrum. and Methods A429(1999)233.
- [11] E.L. Saldin, E.A. Schneidmiller and M.V. Yurkov, Nucl. Instrum. and Methods A490(2002)1.
- [12] Heifets, G. Stupakov and S. Krinsky, Phys. Rev. ST Accel.Beams 5(2002)064401.
- [13] Z. Huang and K.-J. Kim, Phys. Rev. ST Accel.Beams 5(2002)074401.
- [14] Jean-Claude Diels and W. Rudolph, Ultrafast Laser Phenomena, Academic Press, San Diego, 1996.
- [15] P. O'Shea et al., Opt. Lett., vol 26, p. 932(2001).
- [16] P.L. Czonka, Part. Accel.8,225(1978).
- [17] E.L. Saldin, E.A. Schneidmiller and M.V. Yurkov, The physics of Free Electron Lasers, Springer, Berlin-Heidelberg-New-York, 1999.
- [18] B. E. Carlsten, Nucl. Instrum. and Methods A285(1989)313.
- [19] W. S. Graves et al., SLAC-PUB-9440 August 2002.
- [20] D. H. Dowell et al., Nucl. Instrum. and Methods A507(2003)327.
- [21] M. Krasilnikov et al., "Optimizing the PITZ Electron Source for VUV FEL", presented at EPAC 2004, Lucerne, Switzerland, July 2004.